Computationally Efficient Carrier Integer Ambiguity Resolution in GPS/INS: A Common-Position-Shift Approach

Yiming Chen, Sheng Zhao, Jay A. Farrell

***Abstract*—Integer ambiguity resolution is a challenging technical issue that exists in Real-Time Kinematic (RTK) Global Positioning System (GPS) navigation. Once the integer vector is resolved, centimeter-level positioning estimation accuracy can be achieved using the GPS carrier phase measurements. Recently, a real-time, sliding window, Bayesian estimation approach to RTK GPS and inertial navigation was proposed to provide reliable centimeter accurate state estimation, via integer ambiguity resolution utilizing a prior along with all Inertial Measurement Unit (IMU) and GPS measurements within the time window. One challenge to implementing that approach in practice is the high computation cost. This article proposes a novel implementation approach with significantly lower computational requirements and includes a thorough theoretical analysis. Implementation results show that the proposed method resolves an integer vector identical to that of the original method and achieves state estimation with centimeter global positioning accuracy.**

I. Introduction

Integration of GPS and aided inertial navigation systems (INS) has proven useful due to their complementary natures [1]. The INS provides a continuous, high-bandwidth state vector estimate. GPS aiding corrects errors accumulated by the integrative INS process and calibrates the inertial measurement unit (IMU). The overall accuracy of GPS aided INS depends on the accuracy, frequency, and reliability of the GPS measurements. A well-designed GPS receiver typically can reach stand-alone positioning accuracy of $3-8m$ [2]. To reliably achieve higher accuracy positioning, differential GPS (DGPS) is required. With a base station within a range of a few tens of kilometers, DGPS accuracy is on the order of $1m$, growing at the rate of $1m$ per $150km$ of separation [3]. A user can either set up a base station on their own or utilize publicly available correction services: Continuously Operating Reference Station (CORS) [4], Nationwide Differential Global Positioning System (NDGPS) [5], EUREF [6]. As mobile communication networks (4G or WiFi) become readily available, DGPS techniques will become ubiquitous. In this article all GPS measurements are assumed to be processed differentially.

GPS receivers provide carrier phase measurements that are biased by an unknown integer number of wavelengths. While the Phase-Lock-Loop (PLL) of a receiver channel maintains phase lock, the unknown integer for the satellite being tracked remains constant. When loss-of-lock eventually happens (i.e., a cycle-slip occurs), the new integer is most likely to be different. The fundamental ideas underlying integer ambiguity resolution rely on reformulating the problem into an Integer Least Square (ILS) approach, e.g. LAMBDA [7], MLAMBDA [8], or MILES [9]. RTK applications solve the ILS and position estimation problems simultaneously in real-time [10–12]. Solution of the RTK problem is simplified, yet still challenging, when dual-frequency receivers are available, because the integers can be resolved by forming the wide-lane phase measurements [11]. When the integer vector can be resolved, centimeter positioning accuracy is achievable in real-time on moving platforms [13]. The performance of the conventional single-epoch resolution is strongly influence by the number of available satellites, the geometry of the received satellite constellation, and the quality of the measurements. If noisy or faulty measurements exist, the integer resolution can be wrong, without sufficient measurement redundancy to detect the error. For single-frequency receivers, integer ambiguity resolution is even more challenging due to the inability to form the wide-lane measurement and the smaller number (i.e., half) of measurements.

In [14], a Contemplative Real-Time (CRT) approach was proposed to provide a reliable DGPS/INS solution. Within the CRT framework [14–19], the full nonlinear Maximum-a-Posteriori (MAP) estimation problem is solved considering all the information (e.g., prior, kinematics, sensor data) available within a time window [20–23]. The CRT approach provides a large enough set of residuals to extend RAIM techniques [24, 25] to reduce the effects of the outlier measurements on the estimation and to detect incorrect integers. In [17] integer ambiguity resolution is considered within the CRT framework, utilizing graph optimization libraries [26, 27] for the RTK GPS/INS application.

One challenge to implementing reliable integer ambiguity resolution, such as that proposed in [17], is the high computation load, especially when the CRT window is long or the IMU sampling rate is high. This paper considers an alternative implementation approach with significantly lower computational cost. The validity of the approach is demonstrated theoretically and performance is demonstrated experimentally. Implementation results show that the proposed method achieves the centimeter-level global positioning accuracy on moving platforms in challenging GPS environments, gets integer estimates identical to those from the original CRT method.

The outline of this paper is as follows. Section II states the RTK GPS/INS problem. Section III revisited the CRT Integer

Chen, Zhao are Ph.D. students and Farrell is a Professor at the Department of Electrical and Computer Engineering, University of California, Riverside, 92521. {yichen, shzhao, farrell}@ee.ucr.edu.

Ambiguity Resolution proposed in [17]. Section IV presents the proposed *Common-Position-Shift* (CPS) method. Section V analyzes the CPS method mathematically. Section VI presents implementation results. Section VII concludes the paper.

II. Problem Statement

This section presents differential GPS [28] and aided INS [1] background and notation.

A. Aided Inertial Navigation

Let $\boldsymbol{x} \in \mathbb{R}^{n_s}$ denote the rover state vector. For example, the state vector at time t

$$\boldsymbol{x}(t) = [\boldsymbol{p}^\intercal(t), \boldsymbol{v}^\intercal(t), \boldsymbol{q}^\intercal(t), \boldsymbol{b}_a^\intercal(t), \boldsymbol{b}_g^\intercal(t)]^\intercal \in \mathbb{R}^{n_s},$$

is composed of the position, velocity, attitude (e.g., quaternion), accelerometer bias and gyroscope bias vectors.

The kinematic equations for the rover state are

$$\dot{\boldsymbol{x}}(t) = \boldsymbol{f}(\boldsymbol{x}(t), \boldsymbol{u}(t)), \tag{1}$$

where $\boldsymbol{f} : \mathbb{R}^{n_s} \times \mathbb{R}^6 \mapsto \mathbb{R}^{n_s}$ represents the kinematics, and $\boldsymbol{u} \in \mathbb{R}^6$ is the vector of specific forces and angular rates. The function $\boldsymbol{f}$ is accurately known (see Chapter 11 in [1]).

Given a distribution for the initial state $\boldsymbol{x}(t_1) \sim \mathcal{N}(\boldsymbol{x}_1, \mathbf{P}_1)$ where $\boldsymbol{x}_1 \in \mathbb{R}^{n_s}$, $\mathbf{P}_1 \in \mathbb{R}^{n_s \times n_s}$ and measurements $\tilde{\boldsymbol{u}}$ of $\boldsymbol{u}$, the INS propagates the estimate of the rover state between aiding measurement time instants by solving

$$\dot{\hat{\boldsymbol{x}}}(t) = \boldsymbol{f}(\hat{\boldsymbol{x}}(t), \tilde{\boldsymbol{u}}(t)), \tag{2}$$

where $\hat{\boldsymbol{x}}(t)$ denotes the estimate of $\boldsymbol{x}(t)$.

For the convenience of later discussion, define

$$\boldsymbol{s}(t) = [\boldsymbol{v}^\intercal(t), \boldsymbol{q}^\intercal(t), \boldsymbol{b}_a^\intercal(t), \boldsymbol{b}_g^\intercal(t)]^\intercal \in \mathbb{R}^{(n_s-3)} \tag{3}$$

as the state vector excluding the position. Then, we have $\boldsymbol{x}(t) = [\boldsymbol{p}^\intercal(t), \boldsymbol{s}^\intercal(t)]^\intercal$. Similarly, $\boldsymbol{x}_1 = [\boldsymbol{p}_1^\intercal, \boldsymbol{s}_1^\intercal]^\intercal$ for the prior. Similar notation also applies to those of state estimate $\hat{\boldsymbol{x}}(t) = [\hat{\boldsymbol{p}}^\intercal(t), \hat{\boldsymbol{s}}^\intercal(t)]^\intercal$.

Due to prior errors, system calibration errors, and measurement noise, the state estimation error $\delta\boldsymbol{x}(t) = \boldsymbol{x}(t) - \hat{\boldsymbol{x}}(t)$ develops over time. The dynamics and stochastic properties of this estimation error are derived from eqns. (1-2).

When aiding measurements

$$\tilde{\boldsymbol{z}}(t) = \boldsymbol{h}(\boldsymbol{x}(t)) + \boldsymbol{n}_z(t) \tag{4}$$

are available, various methods (e.g., the extended Kalman filter and particle filter) are available to use the initial state, inertial measurements, and aiding measurement information to estimate the rover state vector ([1, 29]).

B. DGPS Measurements

Throughout this article, double-differenced GPS measurements are considered. For notational simplicity, it is assumed that the double difference approach completely removes all common-mode errors (e.g., ionosphere, troposphere, satellite clock and ephemeris), as well as the receiver clock biases, which allows these terms to be dropped throughout the article. This is done only to simplify the notation of the presentation, these errors will still affect the experimental results; therefore, outlier measurements may exist due to multipath error, heavy foliage, receiver failure, etc.

The double-differenced pseudorange (i.e. code) measurement for the $i-$th satellite are modeled as

$$\rho^i(t_k) = h_k^i(\boldsymbol{x}(t_k)) + n_\rho^i(t_k), \tag{5}$$

where $h_k^i(\boldsymbol{x}(t_k)) = \|\boldsymbol{p}(t_k) - \boldsymbol{p}^i(t_k)\|_2$ is the Euclidean distance at t_k between the rover position $\boldsymbol{p} \in \mathbb{R}^3$ and the position of the $i-$th satellite $\boldsymbol{p}^i \in \mathbb{R}^3$, and $n_\rho^i \sim \mathcal{N}(0, \sigma_\rho^2)$ represents the (non-common mode) measurement noise with standard deviation $\sigma_\rho = 0.5 \sim 3m$, depending on receiver design, environmental factors and the performance of multipath mitigation techniques [30]. In practice, the noise level σ_ρ will vary temporally and spatially for each satellite.

The double-differenced carrier phase measurement for the $i-$th satellite is modeled as

$$\varphi^i(t_k) = h_k^i(\boldsymbol{x}(t_k)) + \lambda N^i(t_k) + n_\varphi^i(t_k), \tag{6}$$

where λ is the carrier phase wavelength, and N^i is the unknown integer ambiguity. The measurement noise has distribution $n_\varphi^i \sim \mathcal{N}(0, \sigma_\varphi^2)$. The noise standard deviation σ_φ is millimeter to centimeter level ($< 0.01\sigma_\rho$).

The unknown integer N^i represents the number of carrier wave cycles between the satellite and the receiver at the time that phase-lock is achieved. If the PLL in the receiver for the i-th satellite maintains lock without cycle slips during a time interval $[t_1, t_n]$, then this integer is constant over this time interval, i.e. $N^i(t_1) = \cdots = N^i(t_n) = N^i$. The receiver reports the lock status to enable detection of such time intervals. The unknown integer must be estimated exactly to enable use of the carrier phase measurement for precise position estimation. Note that the carrier phase measurement model does not match the standard measurement model in eqn. (4), because there is a unknown integer variable N^i.

C. Technical Problem Statement

This paper investigates integer ambiguity resolution and trajectory estimation over a time interval $[t_1, t_K]$ that we will refer to as the *CRT window*. This window contains K GPS measurement epochs, where K can be designer specified, time varying, or data dependent. A typical, but simplified,

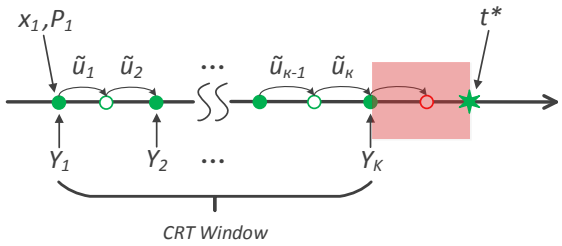

Fig. 1. Illustration of the CRT window measurement time-line. The window contains a prior for the initial state, K GPS measurements, and many IMU measurements between each pair of GPS measurements. All of these items yield constraints on the estimated trajectory $\hat{\boldsymbol{X}}$ during the CRT window.

measurement scenario is depicted in Fig. 1. The dots on the time-line indicate IMU measurement times τ_n. Typically the number of IMU measurements between GPS measurements is very high (i.e. $t_{i+1} - t_i \gg \tau_{j+1} - \tau_j$). This is because IMU sample frequency (e.g., $200Hz$) is at least twice the IMU bandwidth (e.g., $60Hz$), which is higher than the vehicle motion bandwidth (e.g., $10Hz$). The GPS sample rate is usually much lower (e.g., $1.0Hz$). The state transition between these times is constrained by the kinematic model of eqn. (2) and the IMU data. Additional constraints are imposed by the initial estimate $(\boldsymbol{x}_1, \mathbf{P}_1)$ depicted above the initial state, and GPS measurements depicted below the time-line. Each of these constraints is quantified by a probability density which enables a Bayesian estimation formulation for the CRT estimation problem. The computation for the CRT estimation process considering all the information over the CRT window starts at t_K and completes its computation at $t^* > t_K$. This time interval (t_K, t^*) (shown in Fig. 1 with a red zone) is a small fraction of a second with standard off-the-shelf computers. For $t \in (t_K, t^*)$, the real-time state estimate is maintained by the INS. At t^*, the CRT estimation result $\hat{\boldsymbol{x}}(t_K)$ is propagated by the INS with the IMU data over $(t_K, t^*]$ and used to update the real-time estimate. Therefore, the INS is effectively free integrating, without corrections, from t_{K-1} to t^*. For 1 Hz GPS epochs, this duration is significantly less than two seconds and the INS error accumulation is at the centimeter level.

To simplify the presentation of the novel ideas in this paper, the following assumptions are made.

Assumption *1:* Within the CRT window the receiver provides valid carrier phase measurements for m satellites, without loss of lock. △

Assumption *2:* The prior distribution for $\boldsymbol{s}(t_1)$ is $N(\boldsymbol{s}_1, \mathbf{P}_{s_1})$. △

Assumption *3:* The GPS measurement rate is $1Hz$. △

With Assumption 1, the unknown integers in the carrier phase measurements from these m satellites are constants over $[t_1, t_K]$. This assumption will be relaxed in the example section. Assumption 2 allows the system to be initialized at an unknown location, while the partial state estimate $\hat{\boldsymbol{s}}(t_1)$ is initialized with the prior $(\boldsymbol{s}_1, \mathbf{P}_{s_1})$ based on other information sources, while the position is estimated in the CRT window based on GPS. The GPS sampling rate stated in Assumption 3 facilitates the presentation. The entire derivation goes through for other sample rates. Under Assumption 1-3, the CRT estimation problem considered in this paper can be stated as follows.

For a system described by eqn. (1), we have

- an initial distribution for the state $\boldsymbol{s}(t_1) \sim \mathcal{N}(\boldsymbol{s}_1, \mathbf{P}_{s_1})$,
- IMU measurements $\mathbf{U} = \{\mathbf{U}_k\}_{k=1}^{K-1}$, where
$$\mathbf{U}_k = \{\tilde{\boldsymbol{u}}(\tau_n), t_k \le \tau_n \le t_{k+1}\},$$
- DGPS code and carrier phase measurements $\mathbf{Y} = \{\mathbf{Y}_k\}_{k=1}^{K}$, where
$$\mathbf{Y}_k = \{\rho^i(t_k)\}_{i=1}^{m_k} \bigcup \{\varphi^i(t_k)\}_{i=1}^{m}.$$

Note that: $t_1, \ldots, t_k \in (\tau_1, \tau_\kappa]$. The set $\{\tau_n\}_{n=1}^{\kappa}$ contains the high-frequency IMU measurement time instants. The integer m_k is the total number of valid pseudorange measurements at time t_k. For simplicity of discussion in this paper, it is assumed that $m_k \equiv m$. The method presented in this paper can be extended to more complicated mixes of measurements.

Then, the objective is:

Objective *1:* Estimate the optimal state trajectory $\mathbf{X} \triangleq [\boldsymbol{x}^\intercal(t_1), \ldots, \boldsymbol{x}^\intercal(t_K)]^\intercal \in \mathbb{R}^{Kn_s}$ and integers $\mathbf{N} \triangleq [N^1, \ldots, N^m]^\intercal \in \mathbb{Z}^m$ with the given sensor measurements $\mathbf{U}$, $\mathbf{Y}$ and the prior state density $p_{\boldsymbol{s}}(\boldsymbol{s}(t_1))$. △

In [17], the above objective is achieved by formulating and solving the corresponding *Maximum-a-Posteriori* estimation problem. The accuracy and reliability of the solution is achieved by the Nonlinear Mixed Integer Least Square method and faulty data removal scheme. This CRT integer ambiguity resolution method is revisited in Section III to make this paper self-contained.

III. CRT Integer Ambiguity Resolution

Let $\mathbf{X}_+ \triangleq \{\boldsymbol{x}(t) \text{ for } t = t_2, \ldots, t_K\}$, then the joint probability $p(\mathbf{X}, \mathbf{N}, \mathbf{Y}, \mathbf{U})$ can be factored as

$$\begin{aligned}
&p(\mathbf{X}, \mathbf{N}, \mathbf{Y}, \mathbf{U}) \\
&= p(\mathbf{X}, \mathbf{U}, \mathbf{N}) p(\mathbf{Y}|\mathbf{X}, \mathbf{U}, \mathbf{N}) \\
&= p(\mathbf{X}_+, \boldsymbol{x}(t_1), \mathbf{U}) p(\mathbf{Y}|\mathbf{X}, \mathbf{N}) \\
&= p(\boldsymbol{x}(t_1), \mathbf{U}) p(\mathbf{X}_+|\boldsymbol{x}(t_1), \mathbf{U}) p(\mathbf{Y}|\mathbf{X}, \mathbf{N}) \\
&= p(\boldsymbol{x}(t_1)) p(\mathbf{X}_+|\boldsymbol{x}(t_1), \mathbf{U}) p(\mathbf{Y}|\mathbf{X}, \mathbf{N}) \\
&= p(\boldsymbol{s}(t_1)) p(\mathbf{X}_+|\boldsymbol{x}(t_1), \mathbf{U}) p(\mathbf{Y}|\mathbf{X}, \mathbf{N}). \qquad (7)
\end{aligned}$$

For a given prior $(\boldsymbol{s}_1, \mathbf{P}_{s_1})$ and data sets $\mathbf{Y}$ and $\mathbf{U}$, the *Maximum-a-Posteriori* (MAP) trajectory estimate is the $\mathbf{X}$ and $\mathbf{N}$ maximizing the right hand side of eqn. (7):

$$\max_{\mathbf{X} \in \mathbb{R}^{n_s K}, \mathbf{N} \in \mathbb{Z}^m} p(\boldsymbol{s}(t_1)) p(\mathbf{X}_+|\boldsymbol{x}(t_1), \mathbf{U}) p(\mathbf{Y}|\mathbf{X}, \mathbf{N}). \qquad (8)$$

With a Gaussian noise assumption, the negative log-likelihood of the right hand side of eqn. (7) is

$$\begin{aligned}
\|\mathbf{v}(\mathbf{X}, \mathbf{N})\|_{\mathbf{W}}^2 = &\|\boldsymbol{s}(t_1) - \boldsymbol{s}_1\|_{\mathbf{P}_{s_1}}^2 \\
&+ \sum_k \|\boldsymbol{\phi}\big(\boldsymbol{x}(t_k), \mathbf{U}_k\big) - \boldsymbol{x}(t_{k+1})\|_{\mathbf{Q}_k}^2 \\
&+ \sum_k \sum_i \|h_k^i\big(\boldsymbol{x}(t_k)\big) - \rho^i(t_k)\|_{\sigma_\rho^2}^2 \qquad (9) \\
&+ \sum_k \sum_i \|h_k^i\big(\boldsymbol{x}(t_k)\big) + \lambda N^i - \varphi^i(t_k)\|_{\sigma_\varphi^2}^2
\end{aligned}$$

where $\|\mathbf{v}\|_{\mathbf{W}}^2 = \mathbf{v}^\top \mathbf{W}^{-1} \mathbf{v}$ is the squared Mahalanobis distance with matrix $\mathbf{W}$. All terms on the right-hand side also use this notation. The vector $\mathbf{v}$ is the concatenation of each of the vectors summed in the right-hand side of eqn. (9). The operator $\boldsymbol{\phi}$ and the covariance matrix $\mathbf{Q}_k$ used in eqn. (9) are defined in Appendix I. The matrix $\mathbf{W}$ is the positive definite block diagonal matrix formed by the positive definite submatrices $\mathbf{Q}_k$, $\mathbf{P}_{s_1}$, $\sigma_\rho^2 \mathbf{I}$ and $\sigma_\varphi^2 \mathbf{I}$. Using MATLAB syntax, $\mathbf{W}$ could be represented as

$$\mathbf{W} = \text{blkdiag}\big(\mathbf{P}_{s_1}, \mathbf{Q}_0, \ldots, \mathbf{Q}_{K-1}, \sigma_\rho^2 \mathbf{I}, \sigma_\varphi^2 \mathbf{I}\big).$$

Let $\boldsymbol{\Sigma}_W{}^\intercal \boldsymbol{\Sigma}_W = \mathbf{W}^{-1}$, then

$$\boldsymbol{r} \triangleq \boldsymbol{\Sigma}_W \mathbf{v} \qquad (10)$$

is the weighted residual and $\|\mathbf{v}\|^2_{\mathbf{W}} = \|\boldsymbol{r}\|^2$. For notation simplicity, herein we denote the tuple $(\mathbf{X}, \mathbf{N}) = [\mathbf{X}^\intercal, \mathbf{N}^\intercal]^\intercal \in \mathbb{R}^{n_s K} \times \mathbb{Z}^m$. With this notation, the MAP problem is transformed into the Nonlinear Mixed Integer Least Square (NMILS) problem,

$$(\mathbf{X}^*, \mathbf{N}^*) = \underset{\mathbf{X}\in\mathbb{R}^{n_s K}, \mathbf{N}\in\mathbb{Z}^m}{arg\,min} \|\boldsymbol{r}(\mathbf{X}, \mathbf{N})\|^2, \tag{11}$$

where $\boldsymbol{r}$ is the vector:

$$\boldsymbol{r}(\mathbf{X}, \mathbf{N}) = \begin{bmatrix} \boldsymbol{\Sigma}_{\mathbf{P}_{s_1}}(\boldsymbol{s}(t_1) - \boldsymbol{s}_1) \\ \boldsymbol{\Sigma}_{\mathbf{Q}_1}\big(\boldsymbol{\phi}\big(\boldsymbol{x}(t_1), \mathbf{U}_1\big) - \boldsymbol{x}(t_2)\big) \\ \quad\vdots \\ \boldsymbol{\Sigma}_{\mathbf{Q}_{K-1}}\big(\boldsymbol{\phi}\big(\boldsymbol{x}(t_{K-1}), \mathbf{U}_{K-1}\big) - \boldsymbol{x}(t_K)\big) \\ \sigma_\rho^{-1}\big(h_1^1\big(\boldsymbol{x}(t_1)\big) - \rho^1(t_1)\big) \\ \quad\vdots \\ \sigma_\rho^{-1}\big(h_K^m\big(\boldsymbol{x}(t_K)\big) - \rho^m(t_K)\big) \\ \sigma_\varphi^{-1}\big(h_1^1\big(\boldsymbol{x}(t_1)\big) + \lambda N^1 - \varphi^1(t_K)\big) \\ \quad\vdots \\ \sigma_\varphi^{-1}\big(h_K^m\big(\boldsymbol{x}(t_K)\big) + \lambda N^m - \varphi^m(t_K)\big) \end{bmatrix}.$$

The CRT integer ambiguity resolution and trajectory estimation approach from [17] can be summarized with the following three steps:

1) Obtain the *float solution* by neglecting the integral nature of the ambiguity $\mathbf{N}$

$$(\check{\mathbf{X}}, \check{\mathbf{N}}) = \underset{(\mathbf{X},\mathbf{N})\in\mathbb{R}^{n_s K+m}}{arg\,min} \|\boldsymbol{r}(\mathbf{X}, \mathbf{N})\|^2. \tag{12}$$

   Standard outlier rejection techniques [14, 25, 31, 32] can be executed to detect and remove outliers.
2) Starting from $(\check{\mathbf{X}}, \check{\mathbf{N}})$, solve the NMILS problem in eqn. (11) to obtain the optimal solution $(\mathbf{X}^*, \mathbf{N}^*)$.
3) Check the validity of integer estimates with integer validation techniques [33].

The second step of this approach is computationally expensive, especially with relinearization, which requires reintegration. An alternative to the second step is the main focus herein.

To solve the optimization in eqn. (11) in an iterative manner, the *residual* $\boldsymbol{r}(\mathbf{X}, \mathbf{N})$ is linearized around the current estimates $(\hat{\mathbf{X}}, \hat{\mathbf{N}})$:

$$\boldsymbol{r}(\mathbf{X}, \mathbf{N}) \approx \boldsymbol{r}(\hat{\mathbf{X}}, \hat{\mathbf{N}}) + \mathbf{J}(\hat{\mathbf{X}}, \hat{\mathbf{N}})(\delta\mathbf{X}, \delta\mathbf{N}), \tag{13}$$

where $\mathbf{J}(\hat{\mathbf{X}}, \hat{\mathbf{N}})$ is the Jacobian matrix of $\boldsymbol{r}(\mathbf{X}, \mathbf{N})$ evaluated at $(\hat{\mathbf{X}}, \hat{\mathbf{N}})$, and $(\delta\mathbf{X}, \delta\mathbf{N}) = (\mathbf{X}, \mathbf{N}) - (\hat{\mathbf{X}}, \hat{\mathbf{N}})$ is the estimation error. Furthermore, $\mathbf{J}(\hat{\mathbf{X}}, \hat{\mathbf{N}})$ can be decomposed as

$$\mathbf{J}(\hat{\mathbf{X}}, \hat{\mathbf{N}}) = [\mathbf{A}, \mathbf{B}],$$

where $\mathbf{A}$ contains the columns of $\mathbf{J}(\hat{\mathbf{X}}, \hat{\mathbf{N}})$ that are the partial with respect to $\mathbf{X}$ and $\mathbf{B}$ contains the partial with respect to $\mathbf{N}$. Thus, eqn. (13) can be rewritten as

$$\boldsymbol{r}(\mathbf{X}, \mathbf{N}) \approx \boldsymbol{r}(\hat{\mathbf{X}}, \hat{\mathbf{N}}) + \mathbf{A}\delta\mathbf{X} + \mathbf{B}\delta\mathbf{N}.$$

The next step solves the Mixed Integer Least Square (MILES) problem [9]:

$$\min_{\delta\mathbf{X}\in\mathbb{R}^{n_s K}, \delta\mathbf{N}\in\mathbb{Z}^m} \|\boldsymbol{r}(\hat{\mathbf{X}}, \hat{\mathbf{N}}) + \mathbf{A}\delta\mathbf{X} + \mathbf{B}\delta\mathbf{N}\|^2. \tag{14}$$

By dropping the notation $(\hat{\mathbf{X}}, \hat{\mathbf{N}})$ in $\boldsymbol{r}(\hat{\mathbf{X}}, \hat{\mathbf{N}})$ and defining the **QR**-decomposition

$$\mathbf{A} = [\mathbf{Q}_A, \bar{\mathbf{Q}}_A] \begin{bmatrix} \mathbf{R}_A \\ \mathbf{0} \end{bmatrix}, \tag{15}$$

the cost function in eqn. (14) can be factored as

$$\begin{aligned} &\|\boldsymbol{r} + \mathbf{A}\delta\mathbf{X} + \mathbf{B}\delta\mathbf{N}\|^2 \\ &= \left\| \begin{bmatrix} \mathbf{Q}_A^\intercal \\ \bar{\mathbf{Q}}_A^\intercal \end{bmatrix} \boldsymbol{r} + \begin{bmatrix} \mathbf{R}_A \\ \mathbf{0} \end{bmatrix} \delta\mathbf{X} + \begin{bmatrix} \mathbf{Q}_A^\intercal\mathbf{B} \\ \bar{\mathbf{Q}}_A^\intercal\mathbf{B} \end{bmatrix} \delta\mathbf{N} \right\|^2 \\ &= \|\mathbf{Q}_A^\intercal\boldsymbol{r} + \mathbf{R}_A\delta\mathbf{X} + \mathbf{Q}_A^\intercal\mathbf{B}\delta\mathbf{N}\|^2 + \|\bar{\mathbf{Q}}_A^\intercal\boldsymbol{r} + \bar{\mathbf{Q}}_A^\intercal\mathbf{B}\delta\mathbf{N}\|^2. \end{aligned} \tag{16}$$

Note that for any fixed $\delta\mathbf{N}$, the first term on the right hand side of the above equation can be made equal to zero by appropriate choice of $\delta\mathbf{X}$. Thus, solving the following Integer Least Square (ILS) problem yields the optimum of eqn. (14),

$$\min_{\delta\mathbf{N}\in\mathbb{Z}^m} \|\bar{\mathbf{Q}}_A^\intercal\boldsymbol{r} + \bar{\mathbf{Q}}_A^\intercal\mathbf{B}\delta\mathbf{N}\|^2. \tag{17}$$

ILS solution methods are well presented in [7–9, 34–36]. Typically, the ILS solution has two steps: reduction and search. The state-of-the-art reduction method is usually cast as a QRZ-decomposition [37]. The QRZ-decomposition factorizes $\bar{\mathbf{Q}}_A^\intercal\mathbf{B}$ to facilitate the integer search process. Each iteration of the NMILS is computationally expensive and multiple iterations may be required, due to the need for relinearization in eqn. (13) due to changes in $\hat{\mathbf{X}}$.

Increasing the length K of the CRT window enhances both accuracy and reliability at the expense of a higher computational load. Later in Section V-D, the computational load will be summarized in Table I and compared with the CPS algorithm that is developed herein.

The main contribution of this paper is an alternative approach to replace Step 2. The new approach requires a significantly lower computational load. The general method of proof will be to show first that the two approaches would be equivalent if the GPS measurement equations were linear and time invariant. Then to develop bounds on the errors incurred due to the GPS measurement equation nonlinear effects and time variations. By showing that the bounds are small relative to the measurement noise, we present that these errors are irrelevant for practical engineering purposes. The proposed method is inspired by the observation that in practice the optimal solution trajectory $\mathbf{X}^*$ (with integers resolved) is only different from the float solution $\check{\mathbf{X}}$ in terms of a common 3D position error to each state vector in the trajectory (e.g., see Fig. 2). Mathematical analysis in Section V verifies this observation.

IV. Common Position Shift Estimation

This section presents the proposed Common-Position-Shift (CPS) method which is a computationally efficient alternative to the original CRT method revisited in Section III. The key point is to construct a smaller optimization to replace that in Step (2) of Section III. First, the notation for the CPS method is defined.

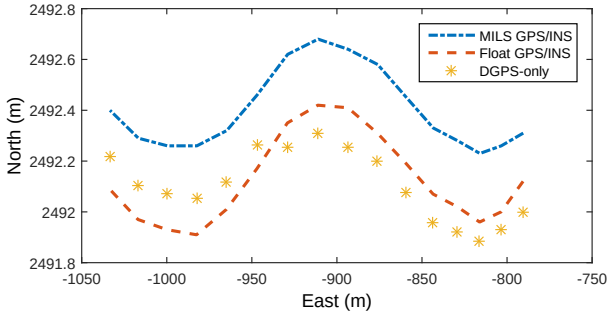

Fig. 2. An example comparison of horizontal positioning results. The dot-dashed (blue) curve is for the MILS GPS/INS solution [17] which has centimeter level accuracy. The dashed (red) curve is for the float solution from eqn. (12). The asterisks (yellow) denote the DGPS (only differential pseudorange, no carrier phase measurements used) positioning solutions.

A. Notation of Common-Position-Shift

Given a trajectory $\mathbf{X} = [\boldsymbol{x}^\intercal(t_1), \ldots, \boldsymbol{x}^\intercal(t_K)]^\intercal$ and a common-position-shift vector $\Delta\boldsymbol{p} \in \mathbb{R}^3$, define the *Common Position Shift* operator $\oplus$ as

$$\mathbf{X}' = \mathbf{X} \oplus \Delta\boldsymbol{p} \triangleq [\boldsymbol{x}^\intercal(t_1) \oplus \Delta\boldsymbol{p}, \ldots, \boldsymbol{x}^\intercal(t_K) \oplus \Delta\boldsymbol{p}]^\intercal$$

which denotes adding the constant vector $\Delta\boldsymbol{p}$ to the position portion, $\boldsymbol{p}(t_k)$, of each state vector $\boldsymbol{x}(t_k)$ in $\mathbf{X}$. The resulting trajectory $\mathbf{X}'$ is referred as the *shifted* trajectory with respect to the original $\mathbf{X}$, see Fig. 3.

B. Outline of the CPS method

This article will show that the cost function $\|\boldsymbol{r}(\mathbf{X}, \mathbf{N})\|^2$ of eqn. (11) can be rewritten as a sum of cost functions:

$$\|\boldsymbol{r}(\mathbf{X}, \mathbf{N})\|^2 = \|\boldsymbol{r}_1(\mathbf{X})\|^2 + \|\boldsymbol{r}_2(\mathbf{X})\|^2 + \|\boldsymbol{r}_3(\mathbf{X}, \mathbf{N})\|^2. \quad (18)$$

These cost functions have two important related properties. First, the term $\|\boldsymbol{r}_1(\mathbf{X})\|^2$ determines the shape, orientation, and general location of the trajectory, but is insensitive to a common position shift $\Delta\boldsymbol{p}$ and to the integer vector $\mathbf{N}$, see Proposition 2. Second, for any given $\mathbf{X}$ the terms $\left(\|\boldsymbol{r}_2(\mathbf{X})\|^2 + \|\boldsymbol{r}_3(\mathbf{X}, \mathbf{N})\|^2\right)$ are independent of $\mathbf{s}$ and can be minimized solely by the choice of $(\Delta\boldsymbol{p}, \mathbf{N})$, see Proposition 3. Therefore, if the linearization errors and the time variation of the GPS measurement model are ignored, Proposition 4 will show that the cost function can be rewritten as

$$\|\boldsymbol{r}(\mathbf{X}, \mathbf{N})\|^2 = \|\boldsymbol{r}_1(\check{\mathbf{X}})\|^2 + \|\boldsymbol{r}_2(\check{\mathbf{X}} \oplus \Delta\boldsymbol{p})\|^2 + \|\boldsymbol{r}_3(\check{\mathbf{X}} \oplus \Delta\boldsymbol{p}, \mathbf{N})\|^2$$

where $\mathbf{X} = \check{\mathbf{X}} \oplus \Delta\boldsymbol{p}$.

These facts allow the problem of interest to be solved by the following approach:

1) Find either the float solution $\check{\mathbf{X}}$ defined in eqn. (12) or the integer free solution $\mathbf{X}^{\circledast}$ defined in eqn. (26), which are shown to be identical in Proposition 1.
2) Find $(\Delta\boldsymbol{p}^\star, \mathbf{N}^\star)$ that is the optimal solution of

$$\min_{\Delta\boldsymbol{p} \in \mathbb{R}^3, \mathbf{N} \in \mathbb{Z}^m} \|\boldsymbol{r}_2(\check{\mathbf{X}} \oplus \Delta\boldsymbol{p})\|^2 + \|\boldsymbol{r}_3(\check{\mathbf{X}} \oplus \Delta\boldsymbol{p}, \mathbf{N})\|^2, \quad (19)$$

where $\check{\mathbf{X}}$ is fixed when evaluating $\|\boldsymbol{r}_2\|^2$+$\|\boldsymbol{r}_3\|^2$.

3) Check the validity of the integer estimates.

The trajectory-integer estimate from the Common-Position-Shift method is finalized as $(\check{\mathbf{X}} \oplus \Delta\boldsymbol{p}^\star, \mathbf{N}^\star)$. The optimality of the solution $(\check{\mathbf{X}} \oplus \Delta\boldsymbol{p}^\star, \mathbf{N}^\star)$ is discussed in Propositions 4 and 5 by comparing with $(\mathbf{X}^*, \mathbf{N}^*)$ obtained from the original NMILS method revisited in Section III.

The Common Position Shift (CPS) estimation in eqn. (19) is designed to replace the original full NMILS Step (2) in Section III. The optimization in eqn. (19) is also solved by the NMILS method outlined in Section III; however, the dimensions are significantly smaller and only a single (linearization) iteration is required.

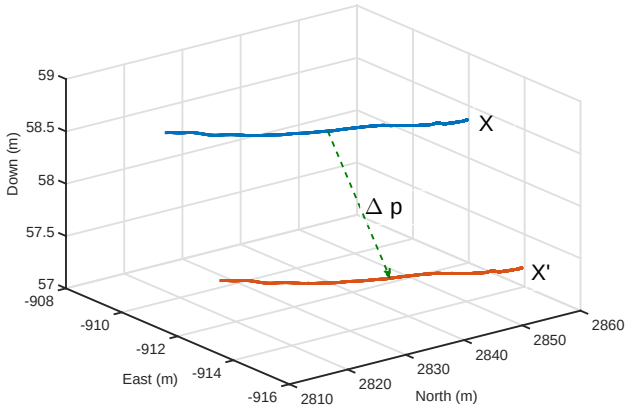

Fig. 3. Example 3D position shift: The blue curve is the original trajectory, the green dashed arrow represents the 3D position shift vector, and the red curve is the shifted trajectory.

C. Decomposition of GPS cost terms

This subsection defines the cost function decomposition for eqn. (18).

Define $\boldsymbol{\varphi}^i = [\varphi^i(t_1), \ldots, \varphi^i(t_K)]^\intercal \in \mathbb{R}^K$ to be the vector stacking the carrier phase measurements of the i-th satellite. The last summation term in eqn. (9) can be rewritten as

$$\begin{aligned} &\sum_k \sum_i \|h_k^i(\boldsymbol{x}(t_k)) + \lambda N^i - \varphi^i(t_k)\|^2_{\sigma_\varphi^2} \\ &= \sum_i \left[\sum_k \|h_k^i(\boldsymbol{x}(t_k)) + \lambda N^i - \varphi^i(t_k)\|^2_{\sigma_\varphi^2} \right] \\ &= \sum_i \|\boldsymbol{h}^i(\mathbf{X}) + \lambda \mathbf{1} N^i - \boldsymbol{\varphi}^i\|^2_{\sigma_\varphi^2 \mathbf{I}}, \end{aligned} \quad (20)$$

where $\boldsymbol{h}^i = [h_1^i(\boldsymbol{x}(t_1)), \ldots, h_K^i(\boldsymbol{x}(t_K))]^\intercal \in \mathbb{R}^K$, $\mathbf{1} = [1, \ldots, 1]^\intercal \in \mathbb{R}^K$, and $\mathbf{I}$ is the $K \times K$ identity matrix. In particular, $\mathbf{1}$ is rank 1 and can be *QR*-decomposed as

$$[\mathcal{Q}_\mathbf{1}, \bar{\mathcal{Q}}_\mathbf{1}] \begin{bmatrix} \mathcal{R}_\mathbf{1} \\ \mathbf{0} \end{bmatrix} = \mathbf{1},$$

where[1] $[\mathcal{Q}_\mathbf{1}^\intercal]_{1 \times K}$ and $[\bar{\mathcal{Q}}_\mathbf{1}^\intercal]_{(K-1) \times K}$ are mappings to the column space and the left null space of $\mathbf{1}$. Let $\mathcal{Q} = [\mathcal{Q}_\mathbf{1}, \bar{\mathcal{Q}}_\mathbf{1}]$,

[1]Note that we use $\mathcal{Q}_\mathbf{1}$ and $\mathbf{Q}_1$ as two different notations: the former represents the column spans the column space of $\mathbf{1}$ while the latter represent the covariance matrix of the first INS cost term in eqn. (9).

which is a unitary matrix. This *QR*-decomposition can be computed offline for different K.

The i-th term in (20) can be decomposed into two parts by projecting it on the column space and the left null space of $\mathbf{1}$,

$$\begin{aligned}
&\|\boldsymbol{h}^i(\mathbf{X}) + \lambda\mathbf{1}N^i - \boldsymbol{\varphi}^i\|^2_{\sigma_\varphi^2\mathbf{I}} \\
&= \left\|\mathcal{Q}^\intercal\left(\boldsymbol{h}^i(\mathbf{X}) + \lambda\mathbf{1}N^i - \boldsymbol{\varphi}^i\right)\right\|^2_{\mathcal{Q}^\intercal\sigma_\varphi^2\mathcal{Q}} \\
&= \left\|\begin{bmatrix}\mathcal{Q}_\mathbf{1}^\intercal \\ \bar{\mathcal{Q}}_\mathbf{1}^\intercal\end{bmatrix}\left[\boldsymbol{h}^i(\mathbf{X}) + \lambda\mathcal{Q}\begin{bmatrix}\mathcal{R}_\mathbf{1} \\ \mathbf{0}\end{bmatrix}N^i - \boldsymbol{\varphi}^i\right]\right\|^2_{\sigma_\varphi^2\mathbf{I}} \\
&= \left\|\begin{bmatrix}\mathcal{Q}_\mathbf{1}^\intercal\boldsymbol{h}^i(\mathbf{X}) + \lambda\mathcal{R}_\mathbf{1}N^i - \mathcal{Q}_\mathbf{1}^\intercal\boldsymbol{\varphi}^i \\ \bar{\mathcal{Q}}_\mathbf{1}^\intercal\left(\boldsymbol{h}^i(\mathbf{X}) - \boldsymbol{\varphi}^i\right)\end{bmatrix}\right\|^2_{\sigma_\varphi^2\mathbf{I}} \\
&= \left\|\bar{\mathcal{Q}}_\mathbf{1}^\intercal\left(\boldsymbol{h}^i(\mathbf{X}) - \boldsymbol{\varphi}^i\right)\right\|^2_{\sigma_\varphi^2\mathbf{I}^-} \\
&\quad + \left\|\mathcal{Q}_\mathbf{1}^\intercal\boldsymbol{h}^i(\mathbf{X}) + \lambda\mathcal{R}_\mathbf{1}N^i - \mathcal{Q}_\mathbf{1}^\intercal\boldsymbol{\varphi}^i\right\|^2_{\sigma_\varphi^2}, \qquad (21)
\end{aligned}$$

where $\mathbf{I}^- = \bar{\mathcal{Q}}_\mathbf{1}^\intercal\bar{\mathcal{Q}}_\mathbf{1}$ is the $(K-1)\times(K-1)$ identity matrix. Note that the first term in eqn. (21) is independent of the integer ambiguity N^i.

Applying the same *QR*-factorization to the pseudorange summation term in eqn. (9) and reorganizing yields:

$$\begin{aligned}
\|\boldsymbol{r}(\mathbf{X},\mathbf{N})\|^2 &= \|\boldsymbol{s}(t_1) - \boldsymbol{s}_1\|^2_{\mathbf{P}_{s_1}} \\
&\quad + \sum_k \|\boldsymbol{\phi}\big(\boldsymbol{x}(t_k),\mathbf{U}_k\big) - \boldsymbol{x}(t_{k+1})\|^2_{\mathbf{Q}_k} \\
&\quad + \sum_i \left\|\bar{\mathcal{Q}}_\mathbf{1}^\intercal\left(\boldsymbol{h}^i(\mathbf{X}) - \boldsymbol{\rho}^i\right)\right\|^2_{\sigma_\rho^2\mathbf{I}^-} \\
&\quad + \sum_i \left\|\bar{\mathcal{Q}}_\mathbf{1}^\intercal\left(\boldsymbol{h}^i(\mathbf{X}) - \boldsymbol{\varphi}^i\right)\right\|^2_{\sigma_\varphi^2\mathbf{I}^-} \qquad (22) \\
&\quad + \sum_i \left\|\mathcal{Q}_\mathbf{1}^\intercal\boldsymbol{h}^i(\mathbf{X}) - \mathcal{Q}_\mathbf{1}^\intercal\boldsymbol{\rho}^i\right\|^2_{\sigma_\rho^2} \\
&\quad + \sum_i \left\|\mathcal{Q}_\mathbf{1}^\intercal\boldsymbol{h}^i(\mathbf{X}) + \lambda\mathcal{R}_\mathbf{1}N^i - \mathcal{Q}_\mathbf{1}^\intercal\boldsymbol{\varphi}^i\right\|^2_{\sigma_\varphi^2}.
\end{aligned}$$

Based on the above expression, it will be convenient to define the following three cost functions. The first cost function:

$$\begin{aligned}
\|\boldsymbol{r}_1(\mathbf{X})\|^2 &\triangleq \|\boldsymbol{s}(t_1) - \boldsymbol{s}_1\|^2_{\mathbf{P}_{s1}} \\
&\quad + \sum_k \left\|\boldsymbol{\phi}\big(\boldsymbol{x}(t_k),\mathbf{U}_k\big) - \boldsymbol{x}(t_{k+1})\right\|^2_{\mathbf{Q}_k} \\
&\quad + \sum_i \left\|\bar{\mathcal{Q}}_\mathbf{1}^\intercal\left(\boldsymbol{h}^i(\mathbf{X}) - \boldsymbol{\rho}^i\right)\right\|^2_{\sigma_\rho^2} \\
&\quad + \sum_i \left\|\bar{\mathcal{Q}}_\mathbf{1}^\intercal\left(\boldsymbol{h}^i(\mathbf{X}) - \boldsymbol{\varphi}^i\right)\right\|^2_{\sigma_\varphi^2\mathbf{I}^-}
\end{aligned}$$

neglects the last two terms in eqn. (22) of $\|\boldsymbol{r}(\mathbf{X},\mathbf{N})\|^2$. The second cost function is

$$\|\boldsymbol{r}_2(\mathbf{X})\|^2 \triangleq \sum_i \left\|\mathcal{Q}_\mathbf{1}^\intercal\boldsymbol{h}^i(\mathbf{X}) - \mathcal{Q}_\mathbf{1}^\intercal\boldsymbol{\rho}^i\right\|^2_{\sigma_\rho^2}. \qquad (23)$$

The third cost function is

$$\|\boldsymbol{r}_3(\mathbf{X},\mathbf{N})\|^2 \triangleq \sum_i \left\|\mathcal{Q}_\mathbf{1}^\intercal\boldsymbol{h}^i(\mathbf{X}) + \lambda\mathcal{R}_\mathbf{1}N^i - \mathcal{Q}_\mathbf{1}^\intercal\boldsymbol{\varphi}^i\right\|^2_{\sigma_\varphi^2} \qquad (24)$$

which will define the common position shift and is analyzed in Section IV-B. With these definitions,

$$\|\boldsymbol{r}(\mathbf{X},\mathbf{N})\|^2 = \|\boldsymbol{r}_1(\mathbf{X})\|^2 + \|\boldsymbol{r}_2(\mathbf{X})\|^2 + \|\boldsymbol{r}_3(\mathbf{X},\mathbf{N})\|^2. \qquad (25)$$

To simplify expressions in the following discussion, let

$$\begin{aligned}
\|\boldsymbol{r}_a(\mathbf{X})\|^2 &\triangleq \|\boldsymbol{r}_1(\mathbf{X})\|^2 + \|\boldsymbol{r}_2(\mathbf{X})\|^2 \\
\|\boldsymbol{r}_b(\mathbf{X},\mathbf{N})\|^2 &\triangleq \|\boldsymbol{r}_2(\mathbf{X})\|^2 + \|\boldsymbol{r}_3(\mathbf{X},\mathbf{N})\|^2.
\end{aligned}$$

D. Integer Free Solution

Define the integer-free solution as

$$\mathbf{X}^\circledast = \underset{\mathbf{X}\in\mathbb{R}^{n_s K}}{arg\,min}\ \|\boldsymbol{r}_a(\mathbf{X})\|^2. \qquad (26)$$

Proposition *1:* If the variable $\mathbf{N}$ is treated as a real vector, then for $\check{\mathbf{X}}$ and $\check{\mathbf{N}}$ as defined in eqn. (12)

$$\|\boldsymbol{r}(\check{\mathbf{X}},\check{\mathbf{N}})\|^2 = \|\boldsymbol{r}_a(\mathbf{X}^\circledast)\|^2$$

and $\mathbf{X}^\circledast = \check{\mathbf{X}}$ where $\boldsymbol{r}(\mathbf{X},\mathbf{N})$ is defined in eqn. (11). △

Proof 1: From eqn. (25),

$$\begin{aligned}
\|\boldsymbol{r}(\mathbf{X},\mathbf{N})\|^2 &= \|\boldsymbol{r}_1(\mathbf{X})\|^2 + \|\boldsymbol{r}_2(\mathbf{X})\|^2 \\
&\quad + \sum_i \left\|\mathcal{Q}_\mathbf{1}^\intercal\boldsymbol{h}^i(\mathbf{X}) + \lambda\mathcal{R}_\mathbf{1}N^i - \mathcal{Q}_\mathbf{1}^\intercal\boldsymbol{\varphi}^i\right\|^2_{\sigma_\varphi^2}.
\end{aligned}$$

Each term in the summation is a scalar:

$$\mathcal{Q}_\mathbf{1}^\intercal\boldsymbol{h}^i(\mathbf{X}) + \lambda\mathcal{R}_\mathbf{1}N^i - \mathcal{Q}_\mathbf{1}^\intercal\boldsymbol{\varphi}^i. \qquad (27)$$

When N^i is treated as a real variable, then for any $\mathbf{X}$ the value

$$\check{N}^i \;=\; \frac{\mathcal{Q}_\mathbf{1}^\intercal\left(\boldsymbol{\varphi}^i - \boldsymbol{h}^i(\mathbf{X})\right)}{\lambda\mathcal{R}_\mathbf{1}} \qquad (28)$$

makes the i-th term zero. Therefore,

$$\|\boldsymbol{r}(\mathbf{X},\check{\mathbf{N}})\| = \|\boldsymbol{r}_1(\mathbf{X})\|^2 + \|\boldsymbol{r}_2(\mathbf{X})\|^2.$$

Proposition 1 indicates that the integer-free solution is equivalent to the float solution of eqn. (12). This equivalence will be utilized in Section V.

V. Common Position Shift Method Analysis

This section presents mathematical analysis of the proposed CPS method. With the aid of several propositions proved herein, the optimality of the CPS method is discussed in Propositions 4 and 5.

A. Useful Constants related to GPS

In the analysis to follow, certain GPS related facts will be used [2, 3, 28]. They are summarized in this paragraph. The standard deviation of the differential pseudorange measurement is $\sigma_\rho = 0.5 \sim 3$ meters. The standard deviation of the differential phase measurement is $\sigma_\varphi \approx 0.01\sigma_\rho$. The minimum distance from a receiver on the earth surface to a GPS satellites satisfies

$$h_k^i\big(\boldsymbol{p}_k\big) = \|\boldsymbol{p}(t_k) - \boldsymbol{p}^i(t_k)\| \geq \underline{D} \triangleq 20000km.$$

The orbital speed of GPS satellite with respect to the ECEF origin satisfies $\|V^i\| \leq \bar{V} \triangleq 4.0km/s$. When the DGPS base station is within a few tens of kilometers, DGPS accuracy is in the order of 1 meter (i.e., 1 σ) [3]. Herein, it is assumed that there are always proprietary or public base stations (e.g. from CORS [4]) available to the rover within $20km$. Therefore, for the float solution $\check{\mathbf{X}}$,

$$\|\check{\boldsymbol{p}}(t_k) - \boldsymbol{p}(t_k)\| < \Delta_f = 3m.$$

B. Propositions for the CPS method

Prop. 2 quantifies the sensitivity of $\|\boldsymbol{r}_1(\hat{\mathbf{X}})\|^2$ to a CPS.

Proposition *2:* For any trajectory estimate $\hat{\mathbf{X}} \in \mathbb{R}^{n_s K}$.

1) Neglecting the time variation and the high-order-terms in the linearization of the GPS measurement model,
$$\|\boldsymbol{r}_1(\hat{\mathbf{X}} \oplus \Delta\boldsymbol{p})\|^2 = \|\boldsymbol{r}_1(\hat{\mathbf{X}})\|^2. \tag{29}$$
2) Accounting for the time variation and the high-order-terms in the linearization of the GPS measurement model, for any trajectory estimate $\hat{\mathbf{X}} \in \mathbb{R}^{n_s K}$ with $\|\Delta p\| < 10km$ it is valid that
$$\bar{\mathcal{Q}}_1^\intercal \left(\boldsymbol{h}^i(\hat{\mathbf{X}} \oplus \Delta\boldsymbol{p}) - \boldsymbol{\varphi}^i\right) = \bar{\mathcal{Q}}_1^\intercal \left(\boldsymbol{h}^i(\hat{\mathbf{X}}) - \boldsymbol{\varphi}^i + \boldsymbol{\delta}_1\right) \tag{30}$$
$$\bar{\mathcal{Q}}_1^\intercal \left(\boldsymbol{h}^i(\hat{\mathbf{X}} \oplus \Delta\boldsymbol{p}) - \boldsymbol{\rho}^i\right) = \bar{\mathcal{Q}}_1^\intercal \left(\boldsymbol{h}^i(\hat{\mathbf{X}}) - \boldsymbol{\rho}^i + \boldsymbol{\delta}_1\right) \tag{31}$$
where $\boldsymbol{\delta}_1 \in \mathbb{R}^K$ is a vector of perturbations caused by the common position shift. Furthermore, the magnitude of $\boldsymbol{\delta}_1$ is bounded by
$$\|\boldsymbol{\delta}_1\|_\infty \leq B_1(\|\Delta\boldsymbol{p}\|, \bar{v}), \tag{32}$$
where the real function $B_1 : \mathbb{R}_+^2 \mapsto \mathbb{R}_+$ is defined as
$$B_1(\|\Delta\boldsymbol{p}\|, \bar{v}) \triangleq K(C_1 + C_2\bar{v})\|\Delta\boldsymbol{p}\| + \|\Delta\boldsymbol{p}\|^2/2\underline{D} \tag{33}$$
and K is the CRT window length in seconds, $C_1 \triangleq \frac{\bar{V}}{\underline{D}} = 2.0 \times 10^{-4}$, $C_2 \triangleq \frac{1}{\underline{D}} = 5.0 \times 10^{-8} s/m$, $\bar{v}$ is the upper bound of the rover speed over the window, and $\|\Delta\boldsymbol{p}\|$ is the magnitude of common position shift.

△

Proof 2: First, a common-position-shift $\Delta\boldsymbol{p}$ will not cause any variation in the prior cost and the INS cost terms, i.e.,
$$\sum_k \left\|\boldsymbol{\phi}\big(\boldsymbol{x}(t_k \oplus \Delta\boldsymbol{p}), \mathbf{U}_k\big) - \boldsymbol{x}(t_{k+1} \oplus \Delta\boldsymbol{p})\right\|_{\mathbf{Q}_k}^2 = \sum_k \left\|\boldsymbol{\phi}\big(\boldsymbol{x}(t_k), \mathbf{U}_k\big) - \boldsymbol{x}(t_{k+1})\right\|_{\mathbf{Q}_k}^2.$$
So, the proof of eqn. (29) focuses on the GPS measurements. Eqn. (30) and (31) are first derived by considering the time variation and the high-order-terms in the linearization of the GPS measurement model, and then by neglecting the perturbation $\boldsymbol{\delta}_1$ due to linearization errors, eqn. (29) can be obtained.

With the assumption $\|\Delta\boldsymbol{p}\| < 10km$, the numerical analysis in Section 8.8.1.3 of [1] show that
$$h_k^i(\boldsymbol{p}_k + \Delta\boldsymbol{p}) - h_k^i(\boldsymbol{p}_k) = H_k^i \Delta\boldsymbol{p} + \frac{\|\Delta\boldsymbol{p}\|^2}{2h_k^i(\boldsymbol{p}_k)} + h.o.t.,$$
where $h_k^i(\boldsymbol{p}_k) = \|\boldsymbol{p}(t_k) - \boldsymbol{p}^i(t_k)\|$ and $H_k^i \in \mathbb{R}^{1\times 3}$ is the Jacobian matrix of h_k^i:
$$H_k^i \triangleq H^i(t_k) = \frac{\partial h_k^i}{\partial \boldsymbol{p}(t_k)} = \left[\frac{\boldsymbol{p}(t_k) - \boldsymbol{p}^i(t_k)}{\|\boldsymbol{p}(t_k) - \boldsymbol{p}^i(t_k)\|}\right].$$
Given that $h_k^i(\boldsymbol{p}_k) \geq \underline{D}$ and $\epsilon_k^i \triangleq \|\Delta\boldsymbol{p}\|^2 / \left(2h_k^i(\boldsymbol{p}_k)\right)$, it follows that
$$h_k^i(\boldsymbol{p}_k + \Delta\boldsymbol{p}) - h_k^i(\boldsymbol{p}_k) = H_k^i \Delta\boldsymbol{p} + \epsilon_k^i, \tag{34}$$
with $|\epsilon_k^i| < \|\Delta\boldsymbol{p}\|^2/2\underline{D}$.

Consider $H^i(t) : \mathbb{R} \mapsto \mathbb{R}^3$ as a function of time,
$$\bar{t} \triangleq (t_K + t_1)/2 \quad \text{and} \quad \bar{H}^i \triangleq H^i(\bar{t}), \tag{35}$$
then by Taylor series, it follows that
$$H^i(t) = \bar{H}^i + \frac{dH^i(t)}{dt}(t - \bar{t}) + h.o.t. \tag{36}$$
By defining the variation
$$\check{H}_k^i \triangleq H_k^i - \bar{H}^i,$$
and using eqn. (36), $\check{H}_k^i$ can be written as
$$\check{H}_k^i = \frac{dH^i(t_k)}{dt}(t_k - \bar{t}) + h.o.t.$$
The derivative $dH^i(t)/dt$ is
$$\frac{dH^i(t_k)}{dt} = \frac{\boldsymbol{v}(t) - \boldsymbol{v}^i(t)}{\|\boldsymbol{p}(t) - \boldsymbol{p}^i(t)\|} - \frac{\big(\boldsymbol{p}(t) - \boldsymbol{p}^i(t)\big)\big(\boldsymbol{p}(t) - \boldsymbol{p}^i(t)\big)^\intercal \big(\boldsymbol{v}(t) - \boldsymbol{v}^i(t)\big)}{\|\boldsymbol{p}(t) - \boldsymbol{p}^i(t)\|^3}; \tag{37}$$
therefore, the variation of the Jacobian matrix is bounded by
$$\|\check{H}_k^i\| \leq \frac{2\left(\bar{v} + \bar{V}\right)}{\underline{D}}|t_k - \bar{t}|,$$
since $\|\boldsymbol{v}(t)\| \leq \bar{v}$ and $\|\boldsymbol{v}^i(t)\| \leq \bar{V}$. Furthermore, with Assumption 3, $(t_K - t_1) < K$ then
$$\left\|\check{H}_k^i\right\| \leq \frac{\bar{V} + \bar{v}}{\underline{D}}(t_K - t_1) = K(C_1 + C_2\bar{v}). \tag{38}$$

We are now in a position to consider the effect of a shift $\Delta\boldsymbol{p}$ on the value of $\bar{\mathcal{Q}}_1^\intercal \boldsymbol{h}^i(\hat{\mathbf{X}} \oplus \Delta\boldsymbol{p})$:
$$\begin{aligned}
&\bar{\mathcal{Q}}_1^\intercal \boldsymbol{h}^i(\hat{\mathbf{X}} \oplus \Delta\boldsymbol{p}) \\
&= \bar{\mathcal{Q}}_1^\intercal \begin{bmatrix} h_1^i(\hat{\boldsymbol{p}}_1 + \Delta\boldsymbol{p}) \\ \vdots \\ h_K^i(\hat{\boldsymbol{p}}_K + \Delta\boldsymbol{p}) \end{bmatrix} \\
&= \bar{\mathcal{Q}}_1^\intercal \begin{bmatrix} h_1^i(\hat{\boldsymbol{p}}_1) + H_1^i\Delta\boldsymbol{p} + \epsilon_1^i \\ \vdots \\ h_K^i(\hat{\boldsymbol{p}}_K) + H_K^i\Delta\boldsymbol{p} + \epsilon_K^i \end{bmatrix} \\
&= \bar{\mathcal{Q}}_1^\intercal \begin{bmatrix} h_1^i(\hat{\boldsymbol{p}}_1) \\ \vdots \\ h_K^i(\hat{\boldsymbol{p}}_K) \end{bmatrix} + \bar{\mathcal{Q}}_1^\intercal \begin{bmatrix} H_1^i \\ \vdots \\ H_K^i \end{bmatrix} \Delta\boldsymbol{p} + \bar{\mathcal{Q}}_1^\intercal \boldsymbol{\epsilon}^i,
\end{aligned}$$
where for ϵ_k^i in eqn. (34)
$$\boldsymbol{\epsilon}^i \triangleq [\epsilon_1^i, \ldots, \epsilon_K^i]^\intercal \in \mathbb{R}^K. \tag{39}$$
With the notation of $\bar{H}^i$ and $\check{H}_k^i$, it follows that
$$\begin{aligned}
&\bar{\mathcal{Q}}_1^\intercal \boldsymbol{h}^i(\hat{\mathbf{X}} \oplus \Delta\boldsymbol{p}) \\
&= \bar{\mathcal{Q}}_1^\intercal \boldsymbol{h}^i(\hat{\mathbf{X}}) + \bar{\mathcal{Q}}_1^\intercal \begin{bmatrix} \check{H}_1^i \\ \vdots \\ \check{H}_K^i \end{bmatrix} \Delta\boldsymbol{p} + \bar{\mathcal{Q}}_1^\intercal \begin{bmatrix} \bar{H}^i\Delta\boldsymbol{p} \\ \vdots \\ \bar{H}^i\Delta\boldsymbol{p} \end{bmatrix} + \bar{\mathcal{Q}}_1^\intercal \boldsymbol{\epsilon}^i \\
&= \bar{\mathcal{Q}}_1^\intercal \left(\boldsymbol{h}^i(\hat{\mathbf{X}}) + \begin{bmatrix} \check{H}_1^i \\ \vdots \\ \check{H}_K^i \end{bmatrix} \Delta\boldsymbol{p} + \boldsymbol{\epsilon}^i \right) + \mathbf{0},
\end{aligned}$$

where the $\mathbf{0}$ term follows from the fact that the columns of $\bar{\mathcal{Q}}_{\mathbf{1}}$ span the left null space of $\mathbf{1}$. Thus, it follows that

$$\bar{\mathcal{Q}}_{\mathbf{1}}^{\intercal}\boldsymbol{h}^i(\hat{\mathbf{X}}\oplus\Delta\boldsymbol{p}) = \bar{\mathcal{Q}}_{\mathbf{1}}^{\intercal}\left[\boldsymbol{h}^i(\hat{\mathbf{X}}) + \boldsymbol{\delta}_1\right] \tag{40}$$

with the perturbation

$$\boldsymbol{\delta}_1 \triangleq \left[\check{H}_1^i\Delta\boldsymbol{p} + \epsilon_1^i, \ldots, \check{H}_K^i\Delta\boldsymbol{p} + \epsilon_K^i\right]^{\intercal}. \tag{41}$$

Then, from eqn. (38) it follows that

$$\begin{aligned}\|\boldsymbol{\delta}_1\|_\infty &= \max\{|\check{H}_k^i\Delta\boldsymbol{p} + \epsilon_1^i|\}\\ &\le K(C_1 + C_2\bar{v})\|\Delta\boldsymbol{p}\| + \|\Delta\boldsymbol{p}\|^2/2\underline{D},\end{aligned}$$

where $C_1 = 2.0\times10^{-4}$ and $C_2 = 5.0\times10^{-8}s/m$.

With eqn. (40), eqn. (30) and (31) can be derived, and then by neglecting the perturbation $\boldsymbol{\delta}_1$, eqn. (29) is valid.

Remark 1: The intuition behind Proposition 2 is that due to the small variation in $\boldsymbol{h}^i(\boldsymbol{p}(t))$, for small time windows and small perturbations $\Delta\boldsymbol{p}$, their effect is removed by the linear transformation $\bar{\mathcal{Q}}^{\intercal}$. For typical values (i.e,, $K \le 10$, $\|\Delta\boldsymbol{p}\| \le 1.5m$, $\bar{v} \le 50m/s$) the upper bound on the perturbation $\|\check{H}_k^i\Delta\boldsymbol{p}\|$ caused by the common position shift is 0.0031 meter, which is a factor of ten smaller than the centimeter noise level of the carrier phase measurement. Because the perturbation is small relative to the carrier phase measurement noise and multipath, they can be neglected. △

Proposition 3 considers the cost functions $\|\boldsymbol{r}_2(\mathbf{X})\|^2$ and $\|\boldsymbol{r}_3(\mathbf{X},\mathbf{N})\|^2$ defined in eqns. (23-24).

Proposition *3:* Consider any two trajectory-integer estimates $(\hat{\mathbf{X}}_1, \hat{\mathbf{N}}_1)$ and $(\hat{\mathbf{X}}_2, \hat{\mathbf{N}}_2)$.

1) Neglecting the time variation and the high-order-terms in the linearization of the GPS measurement model, there exists a correction $(\Delta\boldsymbol{p}, \delta\mathbf{N}) \in \mathbb{R}^3\times\mathbb{Z}^m$ such that

$$\begin{aligned}&\|\boldsymbol{r}_2(\hat{\mathbf{X}}_1\oplus\Delta\boldsymbol{p})\|^2 + \|\boldsymbol{r}_3(\hat{\mathbf{X}}_1\oplus\Delta\boldsymbol{p}, \hat{\mathbf{N}}_1 + \delta\mathbf{N})\|^2\\ &\qquad = \|\boldsymbol{r}_2(\hat{\mathbf{X}}_2)\|^2 + \|\boldsymbol{r}_3(\hat{\mathbf{X}}_2, \hat{\mathbf{N}}_2)\|^2.\end{aligned} \tag{42}$$

2) Define the position errors between trajectories $\hat{\mathbf{X}}_1$ and $\hat{\mathbf{X}}_2$ as $\delta\mathbf{p}_k \triangleq \boldsymbol{p}_k^2 - \boldsymbol{p}_k^1, k = 1,\ldots,K$. Accounting for the time variation and the high-order-terms in the linearization of the GPS measurement model, if $\|\delta\boldsymbol{p}_k\| < 10km$, there exists a correction $(\Delta\boldsymbol{p}, \delta\mathbf{N}) \in \mathbb{R}^3\times\mathbb{Z}^m$ such that

$$\begin{aligned}&\mathcal{Q}_{\mathbf{1}}^{\intercal}\boldsymbol{h}^i(\hat{\mathbf{X}}_1\oplus\Delta\boldsymbol{p}) + \lambda\mathcal{R}_{\mathbf{1}}(\hat{N}_1^i + \delta N^i) - \mathcal{Q}_{\mathbf{1}}^{\intercal}\boldsymbol{\varphi}^i\\ &\qquad = \mathcal{Q}_{\mathbf{1}}^{\intercal}\boldsymbol{h}^i(\hat{\mathbf{X}}_2) + \lambda\mathcal{R}_{\mathbf{1}}\hat{N}_2^i - \mathcal{Q}_{\mathbf{1}}^{\intercal}\boldsymbol{\varphi}^i + \mathcal{Q}_{\mathbf{1}}^{\intercal}\boldsymbol{\delta}_2,\end{aligned} \tag{43}$$

$$\begin{aligned}&\mathcal{Q}_{\mathbf{1}}^{\intercal}\boldsymbol{h}^i(\hat{\mathbf{X}}_1\oplus\Delta\boldsymbol{p}) - \mathcal{Q}_{\mathbf{1}}^{\intercal}\boldsymbol{\rho}^i\\ &\qquad = \mathcal{Q}_{\mathbf{1}}^{\intercal}\boldsymbol{h}^i(\hat{\mathbf{X}}_2) - \mathcal{Q}_{\mathbf{1}}^{\intercal}\boldsymbol{\rho}^i + \mathcal{Q}_{\mathbf{1}}^{\intercal}\boldsymbol{\delta}_2,\end{aligned} \tag{44}$$

where the magnitude of $\boldsymbol{\delta}_2$ is bounded by

$$\|\boldsymbol{\delta}_2\|_\infty \le B_1(\|\Delta\boldsymbol{p}\|, \bar{v}), \tag{45}$$

B_1 is defined in eqn. (33), $\bar{v}$ is the upper bound of the rover speed over the window, and $\|\Delta\boldsymbol{p}\|$ is the magnitude of common position shift.

△

Proof 3: The details of this proof are in Appendix II.

Remark 2: Proposition 3 shows when K and $\|\Delta\boldsymbol{p}\|$ are bounded (e.g. $K \le 10$, $\|\Delta\boldsymbol{p}\| \le 3$ meters), we can minimize $\|\boldsymbol{r}_2(\mathbf{X})\|^2 + \|\boldsymbol{r}_3(\mathbf{X},\mathbf{N})\|^2$ to within a small error, just through a common position shift $\Delta\boldsymbol{p}$ and adjusting the integer estimates by $\delta\mathbf{N}$. Furthermore, the magnitude of the error $\boldsymbol{\delta}_2$ is small relative to the noise level of carrier phase measurements. For example, for $K \le 10$, $\Delta_p \le 1.5$ meters and $\bar{v} \le 50m/s$, it follows that $\|\boldsymbol{\delta}_2\|_\infty \le 0.0031$ meter. △

C. Optimality of the CPS method

The major propositions about the optimality of the CPS method are presented as follows.

Proposition *4:* If $\boldsymbol{\delta}_1 = \mathbf{0}$ and $\boldsymbol{\delta}_2 = \mathbf{0}$, then the following identity is valid,

$$\|\boldsymbol{r}(\check{\mathbf{X}}\oplus\Delta\boldsymbol{p}^\star, \mathbf{N}^\star)\|^2 = \|\boldsymbol{r}(\mathbf{X}^*, \mathbf{N}^*)\|^2, \tag{46}$$

where $\check{\mathbf{X}}$ is the float solution from eqn. (12), $(\Delta\boldsymbol{p}^\star, \mathbf{N}^\star)$ is the CPS solution from eqn. (19) and $(\mathbf{X}^*, \mathbf{N}^*)$ is the full NMILS estimate from eqn. (11). △

Proof 4: See Appendix IV.

Remark 3: This paper and proof introduce different trajectories $\check{\mathbf{X}}$, $\mathbf{X}^*$, $\mathbf{X}^{\circledast}$ and trajectory sets $\mathbf{X}_1^*$, $\mathbf{X}_2^*$ and $\mathbf{X}_\star$. The proof shows that certain components of the cost function have the same value when evaluated for different trajectories or trajectory sets. Taking advantage of this allows definition of the CPS algorithm described in eqn. (19) that vastly reduces the computational load as summarized in Table I. △

Proposition 4 considers the case where the linearization errors do not exist. Proposition 5 analyzes the effect of the linearization errors.

Proposition *5:* Accounting for the time variation and the high-order-terms in the linearization of the GPS measurement model, the following inequality is valid

$$\boldsymbol{E}\{\|\boldsymbol{r}(\check{\mathbf{X}}\oplus\Delta\boldsymbol{p}^\star, \mathbf{N}^\star)\|^2\} \le (1 + C_3)\boldsymbol{E}\{\|\boldsymbol{r}(\mathbf{X}^*, \mathbf{N}^*)\|^2\},$$

where $\check{\mathbf{X}}$ is the float solution from eqn. (12), $(\Delta\boldsymbol{p}^\star, \mathbf{N}^\star)$ is the CPS solution from eqn. (19) with $\|\Delta\boldsymbol{p}^\star\| \le \Delta_f$, and

$$C_3 = \frac{Km\left(4\sigma_\rho^{-2} + 3\sigma_\varphi^{-2}\right)[B_1(\Delta_f, \bar{v})]^2}{(2K-1)m - 3},$$

$(\mathbf{X}^*, \mathbf{N}^*)$ is the full NMILS estimate from eqn. (11) and $\boldsymbol{E}\{\cdot\}$ is the expectation operator. △

Proof 5: See Appendix V.

Remark 4: When $K = 10$, $\Delta_f = 1.5$, $m = 7$, $\sigma_\rho = 1.0$ meters and $\sigma_\varphi = 0.020$ meters, $C_3 = 0.04$. The error between the expected final costs of two optimizations is bounded within 4% of the expected optimum from the full NMILS approach. For the full NMILS solution the residuals at the cm level; therefore, the worst case perturbations would be $0.4mm$. Thus, Propositions 4 and 5 show that the Common Position Shift is a valid and accurate approximation to the original full NMILS approach. △

The implementation results presented in Section VI demonstrates that the differences between two estimation match the expected performance.

D. Computation Analysis of the CPS method

Table I compares the computation costs of the Direct MILS (see Section III) and CPS MILS (see Section IV-A). In Table I, $\mathfrak{I}_1$ represents the number of (linearized) nonlinear least squares iterations required to find in the float solution is Step 1. Similarly, $\mathfrak{I}_2$ represents the number of linearized iterations required for integer ambiguity resolution in the ILS problem of Step 2. The IMU sampling rate (e.g. $200Hz$) is f.

TABLE I
COMPUTATION COMPARISON

Step	Process	Direct MILS	CPS MILS
1)	Float solution	$\mathcal{O}((n_sK)^3) \times \mathfrak{I}_1$	$\mathcal{O}((n_sK)^3) \times \mathfrak{I}_1$
2a)	Integrate INS	$fKn_s \times \mathfrak{I}_2$	0
2b)	QR of A	$2M(N_s)^2 \times \mathfrak{I}_2$	$2(2m)(3)^2 \times \mathfrak{I}_2$
2c)	QRZ of $\bar{\mathbf{Q}}_A^\intercal B$	$2(2Km)m^2 \times \mathfrak{I}_2$	$2(2m)m^2 \times \mathfrak{I}_2$
2d)	Integer Search	$(*) \times \mathfrak{I}_2$	$(*) \times \mathfrak{I}_2$
3)	Integer Valid.	Km	Km

Compared with solving the full NMILS in eqn. (11) directly, the computational cost in eqn. (19) is significantly reduced due to the much smaller dimension of the real unknown variable $\Delta\boldsymbol{p} \in \mathbb{R}^3$ versus $\mathbf{X} \in \mathbb{R}^{n_sK}$. In particular, this dimension reduction facilitates the *QR*-decomposition in eqn. (15), see Row (2b) in Table I. The dimensions of the corresponding A matrices in the full MILS and CPS MILS are $M \times N_s$ versus $2m \times 3$, where $M \triangleq n_sK + 2mK - 3$ is the dimension of the residual vector, $N_s \triangleq n_sK$ is the total state dimension of $\mathbf{X}$, and $2m$ is the total number of GPS measurements at a single epoch (code and carrier phase). Furthermore, while each NMILS iteration of the direct approach requires the expensive INS reintegration, the CPS NMILS of (19) does not, see Row (2a) in Table I. In the ILS, the reduction step is cast as a QRZ-decomposition which is actually a QR factorization with column pivoting (or column reordering) [37]. In CPS MILS, the computation cost on QRZ-decomposition is lower due to the smaller dimension of $\bar{\mathbf{Q}}_A^\intercal B$, see Row (2c) in Table I. On the other hand, the computation of the integer search represented with $(*)$ in Row (2d) of Table I will not vary significantly, since the dimension of $\delta\mathbf{N}$ is the same in both approaches. The computation of the float solution and the integer validation is the same in both the Direct MILS and CPS MILS methods.

TABLE II
EXAMPLE COMPARISON OF COMPUTATIONAL LOAD: $f = 200$, $K = 10$, $n_s = 16$, $N_s = 160$, $M = 297$ AND $m = 7$

Step	Direct MILS	CPS MILS
2a)	$3.20 \times 10^4 \times \mathfrak{I}_2$	0
2b)	$1.52 \times 10^7 \times \mathfrak{I}_2$	$2.52 \times 10^2 \times \mathfrak{I}_2$
2c)	$1.37 \times 10^4 \times \mathfrak{I}_2$	$1.37 \times 10^3 \times \mathfrak{I}_2$

To give a better sense of the computation improvement achieved by the proposed CPS approach, Table II shows an numerical example of computation costs in Row (2a-c) of Table I. In this example, the IMU frequency is $200Hz$, the CRT window length is $K = 10$ epochs, the dimension of navigation state is $n_s = 16$, the average GNSS satellite availability for each epoch is $m = 7$, and then $N_s = 160$, $M = 297$. Table II indicates in each step, the CPS approach saves at least 90% of computation. In particular, the computation cost of the QR decomposition in Step $(2b)$ is significantly reduced by an order of 10^5, if sparsity of matrix A is not exploited in the original Direct MILS approach.

VI. EXPERIMENTS

This section discusses the practical implementations of the proposed CPS method. The computational load has already been discussed. The implementation results in this section demonstrate that the state estimates are close to those of the original approach.

A. Solution Validation

In addition to the integer validation techniques, a threshold Δ_f for the common position shift is also used as a way for sanity check. This threshold can be picked by the designer based on the expected positioning accuracy of the float solution. After the CPS estimation in eqn. (19), if $\|\Delta\boldsymbol{p}^\star\| < \Delta_f$ and $\mathbf{N}^\star$ can be validated with standard integer validation techniques [33], then the estimate of $(\mathbf{X}, \mathbf{N})$ that resulted from this common position shift approach is finalized as $(\check{\mathbf{X}} \oplus \Delta\boldsymbol{p}^\star, \mathbf{N}^\star)$.

Various alternatives are possible if the CPS solution is invalidated. The residuals could be analyzed in an attempt to detect and remove satellites with noisy or invalid measurements, to improve performance within the current epoch. The original full NMILS in eqn. (11) could be executed to attempt to get $(\mathbf{X}^*, \mathbf{N}^*)$. Alternatively, the float solution $\hat{\mathbf{X}}$ could be used to update the real-time state estimates, while at future epochs, the CRT window could be augmented with additional data for the next trial of integer resolution. For example, the designer can choose to slide the current window to the next epoch(s), or extend the length of the current window to accumulate more data. Or, the scheme could just skip the current window and wait for a new window with larger m, which should yield a higher success rate. In the following experiments, $\Delta_f = 3\,m$.

B. Experiments Description

For performance evaluation, the proposed approach is implemented in C++ and applied to RTK GPS/INS data sets collected from an automotive vehicle. The on-vehicle GPS/INS suite consists of a NovAtel OEMV3 receiver which outputs GPS pseudorange and carrier phase measurements at $1Hz$, and a $200Hz$ NV-IMU1000 IMU from NAV Technology Co., Ltd. which outputs the specific forces and angular rate measurements along the three orthogonal axes. The differential GPS information are from the UC Riverside Ntrip caster (ntrip.engr.ucr.edu:2101) which broadcasts raw dual frequency GPS measurements (Message 1004 in RTCM3.1 standard) and the base position (Message 1006 in RTCM3.1 standard) publicly over the internet at $1Hz$ and $0.1Hz$, respectively [38, 39].

Two data sets logged on the vehicle are processed by the CPS approach:

1) a stationary, 12 hours (43200 seconds), data set collected on UC Riverside (UCR) campus, on March 29, 2014;
2) a moving 640 seconds data set collected while driving near the UCR Center for Environmental Research and Technology (CE-CERT), on January 23, 2014.

Since the purpose of the IMU is to cause the residuals to be insensitive to the vehicle motion, the performance (i.e., position error and residual analysis) on the two datasets should be very similar. The accuaracy of the stationary data is much more easily verified. The algorithms were executed on a desktop computer with Intel Core2 Q9400 four-core CPU at 2.66GHz, 8GB DDR3 1333MHz memory, 240GB SSD disk drive. The program runs in Ubuntu 12.04 64-bit OS within a VMware virtual machine for Windows 7. The total memory used by the virtual machine is up to 4 GB. Under this implementation environment and picking the CRT window length $K = 10$ seconds, the average computing time for one CPS iteration is approximately 0.25 ms versus 150 ms for the original full MILS method, indicating significant ($600\times$) computational performance improvement. The code is capable of real-time or post-processed modes of operation. The results presented here are from post-processing, still running in real-time, using stored data.

For the stationary data, the 3D position ground truth is pre-surveyed so positioning errors are presented herein to show the integer ambiguity resolution ability of the CPS method. For the moving data sets, the ground truth is unavailable; therefore, the trajectory and integer estimates from the CPS and the original full MILS method [17] are compared, to show that the CPS is an efficient alternative to the full MILS method, while achieving the same level of accuracy. For both implementations, dual frequency carrier phase measurements are utilized to form wide-lane phase measurements [1]. For both stationary and moving data, histograms of the L1 carrier phase measurements residuals are used as a second method to illustrate CRT accuracy. A 10° elevation mask is applied to GPS satellites. Integers were resolved only when the CRT windows contained at least 5 satellites. In the evaluation of the CPS approach the initial condition and prior term in the cost function of eqn. (9) only include $\boldsymbol{s}$ defined in eqn. (3). There is no prior for the position or integer. Therefore, the integer solution for each CRT window are independent. After estimation at each time step, a residual check is used to validate the integer estimates. If the magnitude of a carrier phase measurement residuals with fixed integer estimate is larger than $0.06\,m$, the integer estimates are rejected. Other integer validation techniques, e.g. ratio test, can be applied [33, 40]. Only validated results are recorded.

C. Stationary Data

For the stationary data, the position of the antenna is surveyed and known with an accuracy at the millimeter level. The algorithm itself has no knowledge of this ground truth position.

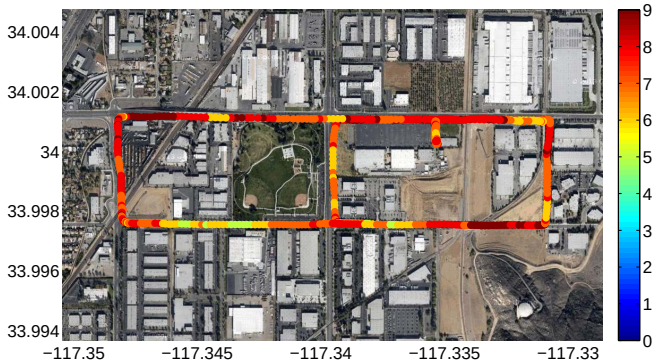

Fig. 5. The route and the satellite availability of the 640s moving data experiment. The x and y axis are the longitude and latitude in degrees. The colors along the route indicate the number of satellites visible to the receiver at that location and time.

For each 10-second CRT windows, the algorithm estimates $\mathbf{X} = [\boldsymbol{x}(t_1)^\intercal, \boldsymbol{x}(t_2)^\intercal, \ldots, \boldsymbol{x}(t_{10})^\intercal]^\intercal$. For the 43200-sec stationary data, 569 trials failed with $m < 5$, 38167 trials are validated (i.e. $m \geq 5$ and the residual check passed). The positioning results are presented through comparison with the ground truth (i.e., $\boldsymbol{p}(t_k) - \boldsymbol{p}_0$ where $\boldsymbol{p}_0$ is the ground truth position). To evaluate the performance of the positioning, the *maximum* norm of the horizontal position error over each CRT window was logged and is shown as a histogram in the upper-left subplot of Fig. 4. Accuracies below $0.02\,m$ are typical, which matches the expected performance of RTK GPS positioning. The lower-left subplot of Fig. 4 shows that the vast majority of the L1 phase residuals lie in $[-0.02, 0.02]\,m$.

D. Moving Data

The route and satellite availability while logging this dataset are shown in Fig. 5. The average vehicle speed is $35\,km/h$.

Since the ground truth is not available for this dataset, the implementation results of the CPS method are compared with those from the original full MILS method [17]. Implementation results show that all the validated integers from CPS are identical to those from the full MILS method. Furthermore, the upper-right subplot of Fig. 4 shows that the maximum norm, during each CRT window, of the horizontal position error between CPS and full MILS are bounded by $0.04\,m$ and typically less than $0.02\,m$. This demonstrates that the CPS method is a good approximation of the full MILS method in terms of integer ambiguity resolution and positioning. The lower-right subplot of Fig. 4 shows that most of the L1 phase measurement residuals lie in $[-0.02, 0.02]\,m$.

The purpose of Fig. 6 is to validate Proposition 2. For the i-th satellite in each time window, defined

$$\Delta\boldsymbol{r}^i \triangleq \bar{\mathcal{Q}}_1^\intercal \left(\boldsymbol{h}^i\left(\check{\mathbf{X}} \oplus \Delta\boldsymbol{p}^\star\right) - \boldsymbol{\varphi}^i\right) - \bar{\mathcal{Q}}_1^\intercal \left(\boldsymbol{h}^i\left(\check{\mathbf{X}}\right) - \boldsymbol{\varphi}^i\right)$$

which is the variation of the integer-free phase measurement residuals (see Proposition 2) caused by the estimated common-position-shift $\Delta\boldsymbol{p}^\star$. Furthermore, $\Delta\boldsymbol{r}^i$ can be rewritten as

$$\Delta\boldsymbol{r}^i = \bar{\mathcal{Q}}_1^\intercal \left(\boldsymbol{h}^i\left(\check{\mathbf{X}} \oplus \Delta\boldsymbol{p}^\star\right) - \boldsymbol{h}^i\left(\check{\mathbf{X}}\right)\right).$$

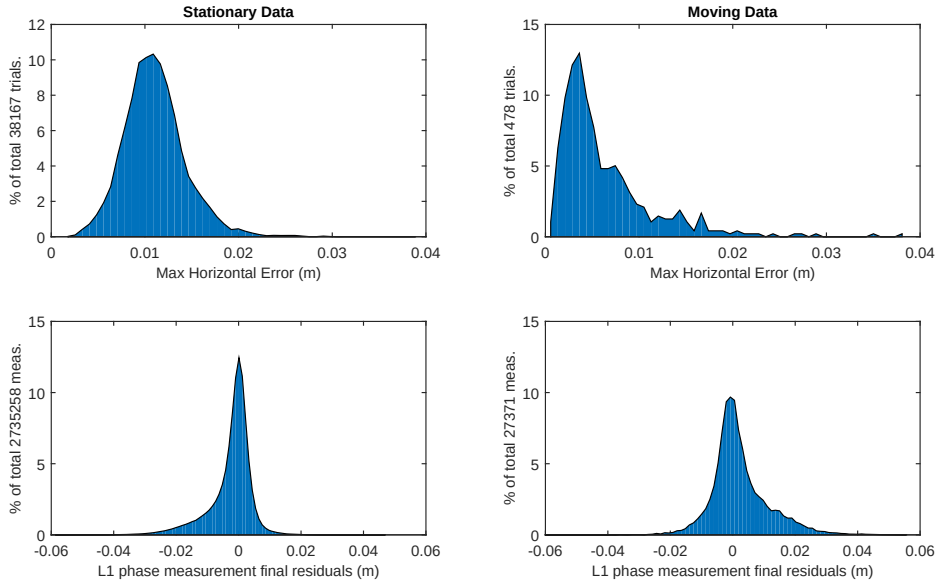

Fig. 4. Maximum norm of horizontal positioning error and posterior L1 phase measurements residuals within each $K = 10$ second CRT window for the Common Position Shift method.

For the moving data, the maximal magnitude of $\Delta \boldsymbol{r}^i$ over each CRT window, i.e.

$$\boldsymbol{\delta}_{max} = \max_i \left\{ \|\Delta \boldsymbol{r}^i\|_\infty \right\}$$

is recorded along with the magnitude of common-position-shift $\|\Delta \boldsymbol{p}^\star\|$ for each CRT window.

Proposition 2 implies that a common-position-shift will only cause small variations, $\Delta \boldsymbol{r}^i$, that are upper-bounded by $B_1(\|\Delta \boldsymbol{p}^\star\|, \bar{v})$. Fig. 6 validates this claim by plotting $\boldsymbol{\delta}_{max}$, $\|\Delta \boldsymbol{p}^\star\|$ and the bound B_1 calculated in eqn. (33). Fig. 6 also shows that in this data set, all the common-position-shift estimates have norm less than 1.2 meter, as expected.

Fig. 7 shows the maximal differences between the CPS estimates and the full MILS estimates of attitude, velocity, bias. Fig. 7 shows that the roll and pitch estimate errors are smaller than 0.1 degree and for yaw angle most of the errors are smaller than 0.5 degree. The velocity estimate errors between two methods are smaller than 0.02 m/s.

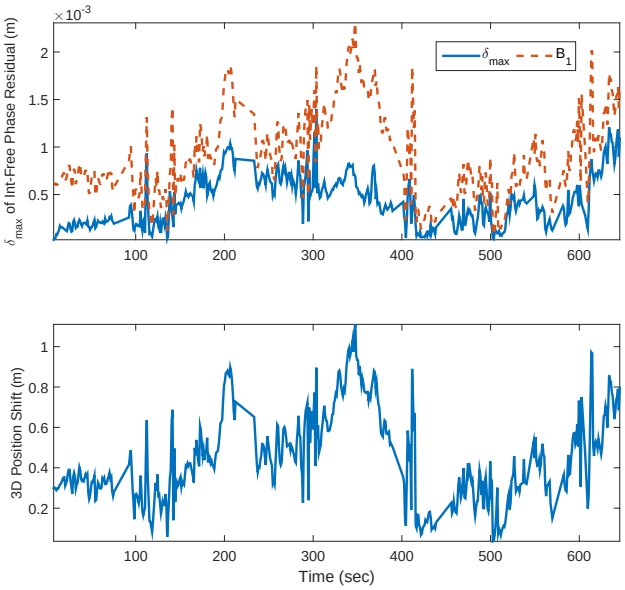

Fig. 6. The magnitude of the 3D position shift estimated by CPS and The variations of $\|\boldsymbol{r}_4\|^2$ caused by the common position shift.

VII. Conclusion

This paper proposes a novel integer ambiguity resolution approach over a time-window of GPS/IMU data. The purpose of processing a window of data is to enhance the reliability of obtaining high-accuracy position estimation, using carrier-phase measurements, even in challenging environments. Enhanced reliability will require further research into outlier detection methods that are beyond the scope of this article.

The CPS method introduced herein has focused on reduction of computational cost. Theoretically the achievable computational savings should be on the order of 10^4, while 600 has been demonstrated. The analysis shows that the estimation accuracy of the original and CPS algorithms would be identical if the GPS measurements were linear and time invariant, and presents bounds on the errors incurred due to the measurement nonlinearity and time dependence.

The theoretical approach is also interesting in that it shows that the cost function can be decomposed into one part that determines the shape and vicinity of the trajectory, but is insensitive to the carrier phase integers and a position shift vector; and, a second part that is sensitive to the carrier phase integer and can be solved to determine the required position shift so that the location of the trajectory is accurately known.

Theoretical analysis is presented for the CPS method. Imple-

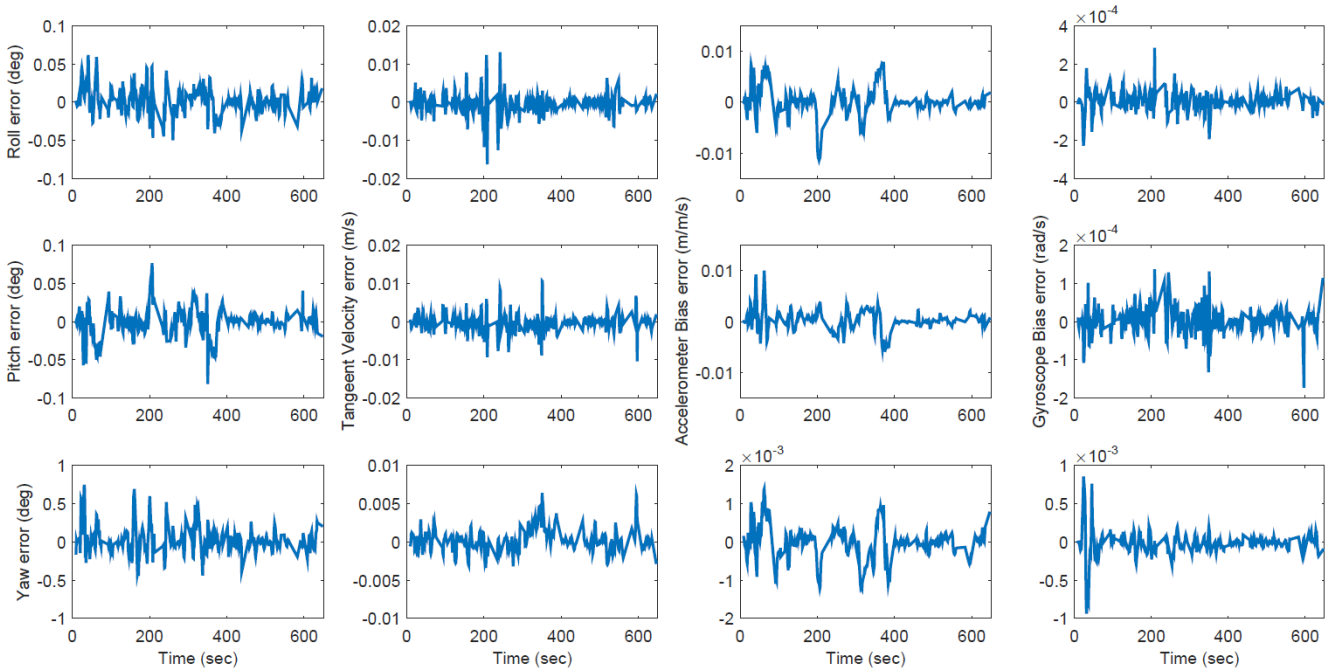

Fig. 7. Max attitude, velocity, bias estimation errors between CPS and full MILS results of the moving data

mentation results show that the proposed CPS method obtains integer estimates identical to those from the original full MILS method, obtains centimeter positioning accuracy, and that other state estimation errors are small.

VIII. Acknowledgments

This research builds on the software [41–46] of and technical conversations with A. I. Mourikis and M. Li also of UC-Riverside. These technical collaborations are greatly appreciated. This research was supported in part by 2013/2014 UCTC Dissertation award.

References

[1] J. A. Farrell, *Aided Navigation: GPS with High Rate Sensors*. McGraw Hill, 2008.

[2] Anonymous, "Global positioning system standard positioning service performance standard," U.S. Department of Defense, Tech. Rep., 2008.

[3] E. Kaplan and C. Hegarty, *Understanding GPS Principles and Applications, 2nd Ed.* Artch House, 2006.

[4] R. A. Snay and M. Tomás Soler, "Continuously operating reference station (CORS): History, applications, and future enhancements," *Journal of Surveying Engineering*, vol. 134, no. 4, pp. 95–104, 2008.

[5] P. Gary and C. E. Fly, "NDGPS assessement final report," U.S. Department of Transportation, Tech. Rep., 2008.

[6] D. Dettmering and G. Weber, "The EUREF-IP NtripBroadcaster: Real-time GNSS data for Europe," in *Proceedings of the IGS Workshop*, Astronimical Institute University of Bern, Switzerland, 2004, pp. 1–8.

[7] P. Jonge and C. Tiberius, "The LAMBDA Method for Integer Ambiguity Estimation: Implementation Aspects," TUDelft, Tech. Rep., 1996.

[8] X. W. Chang, X. Yang, and T. Zhou, "MLAMBDA: a Modified LAMBDA Method for Integer Least-Squares Estimation," *Journal of Geodesy*, vol. 79, no. 9, pp. 552–565, 2005.

[9] X. Chang and T. Zhou, "MILES: MATLAB Package for Solving Mixed Integer LEast Squares Problems," *GPS Solution*, vol. 11, no. 4, pp. 289–294, 2007.

[10] R. Hatch, "The synergism of GPS code and carrier measurements," in *International Geodetic Symposium on Satellite Doppler Positioning, 3rd*, vol. 2, 1983, pp. 1213–1231.

[11] R. Hatch, "Instantaneous ambiguity resolution," in *Symposium No. 107, Kinematic Systems in Geodesy, Surveying and Remote Sensing*. Springer Verlag, 1990, pp. 299–308.

[12] T. Takasu and A. Yasuda, "Development of the Low-cost RTK-GPS Receiver with an Open Source Program Package RTKLIB," in *International Symposium on GPS/GNSS, International Convention Center Jeju, Korea*, 2009, pp. 1–8.

[13] J. Farrell, T. Givargis, and M. Barth, "Real-time Differential Carrier Phase GPS-aided INS," *IEEE Trans. CST*, vol. 8, no. 4, pp. 709–721, 2000.

[14] S. Zhao, Y. Chen, H. Zhang, and J. Farrell, "Differential GPS Aided Inertial Navigation: a Contemplative Realtime Approach," in *the Proceedings of the 19th IFAC World Congress*, Cape Town, South Africa, August 2014, pp. 8959–8964.

[15] Y. Chen, D. Zheng, P. M. Miller, and J. Farrell, "Underwater Vehicle Near Real Time State Estimation," in *the Proceedings of the IEEE Multi-Conference on Systems and Control*, Hyderabad, India, August 2013, pp. 545–550.

[16] ——, "Underwater Inertial Navigation with Long Base Line Transceivers: A Near-Real-Time Approach," in *the Proceedings of the IEEE Conference on Decision and Control*, Florence, Italy, December 2013, pp. 5042–5047.

[17] Y. Chen, S. Zhao, D. Zheng, and J. Farrell, "High Reliability Integer Ambiguity Resolution of 6DOF RTK GPS/INS," in *the Proceedings of the IEEE Conference on Decision and Control*, Los Angeles, December 2014.

[18] Y. Chen, D. Zheng, P. M. Miller, and J. Farrell, "Underwater Inertial Navigation with Long Base Line Transceivers: A Near-Real-Time Approach," *IEEE Trans. on Control Systems Technology (accepted)*, 2014.

[19] S. Zhao, Y. Chen, H. Zhang, and J. Farrell, "High Precision 6DOF Vehicle Navigation in Urban Environments using a Low-cost Single-frequency GPS Receiver," in *the Proceedings of IROS/PPNIV*, Chicago, September 2014, pp. 1–6.

[20] F. Dellaert and M. Kaess, "Square Root SAM: Simultaneous Localization and Mapping via Square Root Information Smoothing," *Int. J. Rob. Res.*, vol. 25, no. 12, pp. 1181–1203, 2006.

[21] M. Kaess, A. Ranganathan, and F. Dellaert, "iSAM: Incremental

Smoothing and Mapping," *IEEE Trans. on Robotics*, vol. 24, no. 6, pp. 1365–1378, 2008.
[22] M. Kaess and F. Dellaert, "Covariance recovery from a square root information matrix for data association," *Journal of Robotics and Autonomous Systems*, 2009.
[23] M. Kaess, H. Johannsson, R. Roberts, V. Ila, J. Leonard, and F. Dellaert, "iSAM2: Incremental smoothing and mapping using the Bayes tree," *Intl. J. of Robotics Research*, vol. 31, no. 2, pp. 216–235, Feb. 2012.
[24] S. Hewitson, H. K. Lee, and J. Wang, "Localizability Analysis for GPS/Galileo Receiver Autonomous Integrity Monitoring," *J. of Navigation*, vol. 57, pp. 245–259, 2004.
[25] S. Hewitson and J. Wang, "Extended Receiver Autonomous Integrity Monitoring (eRAIM) for GNSS/INS Integration," *Journal of Surveying Eng.*, vol. 136, no. 1, pp. 13–22, 2010.
[26] R. Kuemmerle, G. Grisetti, H. Strasdat, K. Konolige, and W. Burgard, "g2o: a General Framework for Graph Optimization," in *Proc. ICRA*, 2011, pp. 3607 – 3613.
[27] F. Dellaert, "Factor Graphs and GTSAM: A Hands-on Introduction," Georgia Institute of Technology, Tech. Rep., 2012.
[28] P. Misra and P. Enge, *GPS: Signals, Measurements, and Performance*. Ganga-Jamma Press, 2001.
[29] S. M. Kay, *Fundamentals of Statistical Signal Processing, Estimation theory*. Prentice Hall PTR, 1993.
[30] X. Chen, F. Dovis, S. Peng, and Y. Morton, "Comparative studies of gps multipath mitigation methods performance," *Aerospace and Electronic Systems, IEEE Transactions on*, vol. 49, no. 3, pp. 1555–1568, July 2013.
[31] P. J. Huber, "Robust Estimation of a Location Parameter," *The Annals of Mathematical Statistics*, 1964.
[32] D. Wang, H. Lu, and M.-H. Yang, "Least soft-threshold squares tracking," *2013 IEEE Conference on Computer Vision and Pattern Recognition*, pp. 2371–2378, Jun. 2013.
[33] S. Verhagen, *The GNSS Integer Ambiguities: Estimation and Validation*. NCG, Nederlandse Commissie voor Geodesie, Netherlands Geodetic Commission, 2005.
[34] P. J. G. Teunissen, "Least-Squares Estimation of the Integer GPS Ambiguities," in *Invited lecture, Section IV: Theory and Methodology*. IAG General Meeting, Beijing, China., 1993, pp. 1–16.
[35] P. Teunissen, "The Least-Squares Ambiguity Decorrelation Adjustment: a Method for Fast GPS Ambiguity Estitmation," *Journal of Geodesy*, vol. 70, pp. 65–82, 1995.
[36] ——, "An Optimality Property of the Integer Least-Squares Estimator," *Journal of Geodesy*, vol. 73, pp. 587–593, 1999.
[37] X. Chang and G. H. Golub, "Solving Ellipsoid-Constrained Integer Least Squares Problems," *SIAM J. MATRIX ANAL. APPL.*, vol. 31, no. 3, pp. 1071–1089, 2009.
[38] RTCM Special Committee No. 104, "RTCM Standard 10403.1, Differential GNSS Services, Version 3," Radio Technical Commission for Maritime Services, Tech. Rep., 2011.
[39] P. Gary and C. E. Fly, "RTCM Standard 10410.1, Networked Transport of RTCM via Internet Protocol (Ntrip), Version 2.0," Radio Technical Commission for Maritime Services, Tech. Rep., 2011.
[40] A. Vu, J. Farrell, and M. Barth, "Centimeter-Accuracy Smoothed Vehicle Trajectory Estimation," *Intelligent Transportation Systems Magazine, IEEE*, vol. 5, no. 4, pp. 121–135, 2013.
[41] T.-C. Dong-Si and A. I. Mourikis, "Motion Tracking with Fixed-lag Smoothing: Algorithm and Consistency Analysis," in *IEEE ICRA*, 2011, pp. 5655–5662.
[42] M. Li and A. I. Mourikis, "Improving the accuracy of EKF-based visual-inertial odometry," in *Proceedings of the IEEE International Conference on Robotics and Automation*, St Paul, MN, May 2012, pp. 828–835.
[43] ——, "Vision-aided inertial navigation for resource-constrained systems," in *Proceedings of the IEEE/RSJ International Conference on Intelligent Robots and Systems*, Vilamoura, Portugal, Oct. 2012, pp. 1057–1063.
[44] M. Li, B. Kim, and A. I. Mourikis, "Real-time motion estimation on a cellphone using inertial sensing and a rolling-shutter camera," in *Proceedings of the IEEE International Conference on Robotics and Automation*, Karlsruhe, Germany, May 2013, pp. 4697–4704.
[45] M. Li, H. Yu, X. Zheng, and A. I. Mourikis, "High-fidelity sensor modeling and self-calibration in vision-aided inertial navigation," in *Proceedings of the IEEE International Conference on Robotics and Automation*, Hong Kong, June 2014, pp. 409–416.
[46] M. Li and A. I. Mourikis, "High-precision, consistent EKF-based visual-inertial odometry," *International Journal of Robotics Research*, vol. 32, no. 6, pp. 690–711, May 2013.
[47] E. M. Mikhail and F. E. Acherman, *Observations and Least Squares*. Univ Pr of Amer, 1976.

Y. Chen received a B.Eng. degree in automation from Tianjin University, Tianjin, China in 2009, M.S. degrees in electrical engineering and mathematics from the University of California at Riverside (UCR) in 2011 and 2013, respectively, and a Ph.D. degree in electrical engineering from (UCR) in 2014. He is currently a Senior Engineer with Qualcomm Research at San Diego, CA. His current research interests include state estimation, optimization, computer vision, machine learning, navigation and automatic control, especially their applications in mobile robots and autonomous vehicles.

S. Zhao received the B.Eng. degree in automation from the Xiamen University, Xiamen, China in 2005, and the Ph.D. degree in electrical engineering from UCR in 2014. He is currently a Senior Computer Vision Engineer at Magic Leap, Inc. His research interests include aided inertial navigation systems for robots, autonomous vehicles and mobile devices, state estimation, and simultaneous localization and mapping.

J. A. Farrell earned B.S. degrees in physics and electrical engineering from Iowa State University, and M.S. and Ph.D. degrees in electrical engineering from the University of Notre Dame. After working at Draper Lab (1989-1994), he joined UCR. He is a Professor and two time Chair of the Department of Electrical and Computer Engineering. He has served the IEEE Control Systems Society on their Board of Governors for two terms, as Vice President Finance and Vice President of Technical Activities, as General Chair for IEEE CDC 2012, and as President in 2014. He is a Fellow of the IEEE, a Fellow of AAAS, a Distinguished Member of IEEE CSS, and author of over 250 technical articles and three books.

APPENDIX

APPENDIX I: INS REVIEW

For any initial state $\boldsymbol{x}(\tau_k)$, the solution to (1) for $t \in [\tau_k, \tau_{k+1}]$ is

$$\boldsymbol{x}(t) = \boldsymbol{x}(\tau_k) + \int_{\tau_k}^{t} \boldsymbol{f}(\boldsymbol{x}(\tau), \boldsymbol{u}(\tau))d\tau. \tag{47}$$

While nature solves (47) in continuous time, the INS only has IMU and aiding measurements at discrete time instants; therefore, the INS numerically solves

$$\begin{aligned}\hat{\boldsymbol{x}}(\tau_{k+1}) &= \boldsymbol{\phi}\big(\hat{\boldsymbol{x}}(\tau_k), \tilde{\boldsymbol{u}}(\tau_k)\big) \\ &= \hat{\boldsymbol{x}}(\tau_k) + \int_{\tau_k}^{\tau_{k+1}} \boldsymbol{f}(\hat{\boldsymbol{x}}(\tau), \tilde{\boldsymbol{u}}(\tau))d\tau,\end{aligned} \tag{48}$$

where $\boldsymbol{\phi}$ is defined as the integration operator. The result of the numeric integration of (48) is the INS state estimate of $\hat{\boldsymbol{x}}(\tau_{k+1})$ given $\hat{\boldsymbol{x}}(\tau_k)$ and $\hat{\boldsymbol{u}}(\tau_k)$. The numeric integration repeats to propagate the state measurements between the times of aiding measurements. The aiding measurement times can be unequally spaced in time without causing any complications.

Let $\tilde{\mathbf{U}}_j = \{\tilde{\boldsymbol{u}}(\tau_k),\ \tau_k \in [t_j, t_{j+1}]\}$, then eqn. (48) can be called recursively to compute $\hat{\boldsymbol{x}}(t_{j+1})$ from $\hat{\boldsymbol{x}}(t_j)$ and $\tilde{\mathbf{U}}_j$, denote this as

$$\hat{\boldsymbol{x}}(t_{j+1}) = \boldsymbol{\phi}\big(\hat{\boldsymbol{x}}(t_j), \tilde{\mathbf{U}}_j\big). \tag{49}$$

At the same time, nature is integrating eqn. (47) which it denoted as

$$\boldsymbol{x}(t_{j+1}) = \boldsymbol{\phi}\big(\boldsymbol{x}(t_j), \mathbf{U}_j\big). \tag{50}$$

The linearized error growth model is

$$\delta\hat{\boldsymbol{x}}(t_{j+1}) = \boldsymbol{\Phi}_j \delta\hat{\boldsymbol{x}}(t_j) + \boldsymbol{\omega}_j \tag{51}$$

where $\boldsymbol{\omega}_j \sim N(0, \mathbf{Q}_j)$ and $\boldsymbol{\Phi}_j = \left.\frac{\partial \boldsymbol{\phi}(\boldsymbol{x})}{\partial \boldsymbol{x}}\right|_{(\hat{\boldsymbol{x}}(t_j), \tilde{\mathbf{U}}_j)}$. The INS provides both $\mathbf{Q}_j$ and $\boldsymbol{\Phi}_j$, see Section 7.2.5.2 in [1].

APPENDIX II

This appendix proves Proposition 3.

Proof 6: The linearization error term $\boldsymbol{\epsilon}^i$ is not included in this proof, but can be added by following the idea in the proof of Proposition 2.

The proof first shows the existence of $(\Delta\boldsymbol{p}, \mathbf{N})$ for eqn. (43) and (44), then allows $\boldsymbol{\delta}_2 = 0$ to prove the existence of $(\Delta\boldsymbol{p}, \mathbf{N})$ for eqn. (42).

From its definition in Section IV, $\mathcal{Q}_{\mathbf{1}}$ is a unit column matrix whose column spans the range space of $\mathbf{1} = [1, \ldots, 1]^\intercal \in \mathbb{R}^K$, i.e.

$$\mathcal{Q}_{\mathbf{1}}^\intercal = [1/\sqrt{K}, \ldots, 1/\sqrt{K}] \in \mathbb{R}^K.$$

Therefore,

$$\mathcal{Q}_{\mathbf{1}}^\intercal \begin{bmatrix} \bar{H}^i \\ \vdots \\ \bar{H}^i \end{bmatrix} = \sqrt{K}\bar{H}^i \tag{52}$$

for the row vector $\bar{H}^i$ as defined in eqn. (35).

Starting from eqn. (43) our goal is to show that there exists $\Delta\boldsymbol{p} \in \Re^3$ and integer δN^i for $i = 1, \ldots, m$, such that

$$\begin{aligned}\mathcal{Q}_{\mathbf{1}}^\intercal \boldsymbol{h}^i\big(\hat{\mathbf{X}}_1 \oplus \Delta\boldsymbol{p}\big) + \lambda\mathcal{R}_{\mathbf{1}}(\hat{N}_1^i + \delta N^i) \\ = \mathcal{Q}_{\mathbf{1}}^\intercal \boldsymbol{h}^i\big(\hat{\mathbf{X}}_2\big) + \lambda\mathcal{R}_{\mathbf{1}} N_2^i + \mathcal{Q}_{\mathbf{1}}^\intercal \boldsymbol{\delta}_2.\end{aligned} \tag{53}$$

Let $\delta\mathbf{X} \triangleq \hat{\mathbf{X}}_2 - \hat{\mathbf{X}}_1$ and $\hat{\boldsymbol{p}}_k \in \mathbb{R}^3$ be the position estimates in $\hat{\mathbf{X}}_1$, then

$$\begin{aligned}
&\mathcal{Q}_{\mathbf{1}}^\intercal \boldsymbol{h}^i\big(\hat{\mathbf{X}}_2\big) && (54)\\
&= \mathcal{Q}_{\mathbf{1}}^\intercal \boldsymbol{h}^i\big(\hat{\mathbf{X}}_1 + \delta\mathbf{X}\big) && (55)\\
&= \mathcal{Q}_{\mathbf{1}}^\intercal \begin{bmatrix} h_1^i(\hat{\boldsymbol{p}}_1 + \Delta\boldsymbol{p}_1) \\ \vdots \\ h_K^i(\hat{\boldsymbol{p}}_K + \Delta\boldsymbol{p}_K) \end{bmatrix} && (56)\\
&= \mathcal{Q}_{\mathbf{1}}^\intercal \begin{bmatrix} h_1^i(\hat{\boldsymbol{p}}_1) \\ \vdots \\ h_K^i(\hat{\boldsymbol{p}}_K) \end{bmatrix} + \mathcal{Q}_{\mathbf{1}}^\intercal \begin{bmatrix} H_1^i\Delta\boldsymbol{p}_1 \\ \vdots \\ H_K^i\Delta\boldsymbol{p}_K \end{bmatrix} && (57)\\
&= \mathcal{Q}_{\mathbf{1}}^\intercal \begin{bmatrix} h_1^i(\hat{\boldsymbol{p}}_1) \\ \vdots \\ h_K^i(\hat{\boldsymbol{p}}_K) \end{bmatrix} + \mathcal{Q}_{\mathbf{1}}^\intercal \begin{bmatrix} \bar{H}^i\Delta\boldsymbol{p}_1 \\ \vdots \\ \bar{H}^i\Delta\boldsymbol{p}_K \end{bmatrix} + \mathcal{Q}_{\mathbf{1}}^\intercal \begin{bmatrix} \check{H}_1^i\Delta\boldsymbol{p}_1 \\ \vdots \\ \check{H}_K^i\Delta\boldsymbol{p}_K \end{bmatrix} && (58)\\
&= \mathcal{Q}_{\mathbf{1}}^\intercal \begin{bmatrix} h_1^i(\hat{\boldsymbol{p}}_1) \\ \vdots \\ h_K^i(\hat{\boldsymbol{p}}_K) \end{bmatrix} + \frac{\bar{H}^i}{\sqrt{K}} \sum_k \Delta\boldsymbol{p}_k + \mathcal{Q}_{\mathbf{1}}^\intercal \begin{bmatrix} \check{H}_1^i(\Delta\boldsymbol{p} + \Delta\check{\boldsymbol{p}}_1) \\ \vdots \\ \check{H}_K^i(\Delta\boldsymbol{p} + \Delta\check{\boldsymbol{p}}_K) \end{bmatrix}
\end{aligned}$$

where $\bar{H}^i$ is the average of Jacobian matrix H_k^i. Define

$$\Delta\boldsymbol{p} = \frac{1}{K}\sum_{i=1}^K \Delta\boldsymbol{p}_k \in \mathbb{R}^3 \tag{59}$$

as the average of the position adjustments in $\delta\mathbf{X}$ and $\Delta\check{\boldsymbol{p}}_k = \Delta\boldsymbol{p}_k - \Delta\boldsymbol{p}$ as the variation of the position adjustments. Continuing, using eqn. (59) and then (52):

$$\begin{aligned}
&\mathcal{Q}_{\mathbf{1}}^\intercal \boldsymbol{h}^i\big(\hat{\mathbf{X}}_2\big) \\
&= \mathcal{Q}_{\mathbf{1}}^\intercal \begin{bmatrix} h_1^i(\hat{\boldsymbol{p}}_1) \\ \vdots \\ h_K^i(\hat{\boldsymbol{p}}_K) \end{bmatrix} + \sqrt{K}\bar{H}^i\Delta\boldsymbol{p} + \mathcal{Q}_{\mathbf{1}}^\intercal \begin{bmatrix} \check{H}_1^i(\Delta\boldsymbol{p} + \Delta\check{\boldsymbol{p}}_1) \\ \vdots \\ \check{H}_K^i(\Delta\boldsymbol{p} + \Delta\check{\boldsymbol{p}}_K) \end{bmatrix} \\
&= \mathcal{Q}_{\mathbf{1}}^\intercal \begin{bmatrix} h_1^i(\hat{\boldsymbol{p}}_1) \\ \vdots \\ h_K^i(\hat{\boldsymbol{p}}_K) \end{bmatrix} + \mathcal{Q}_{\mathbf{1}}^\intercal \begin{bmatrix} (\bar{H}^i + \check{H}_1^i)\Delta\boldsymbol{p} \\ \vdots \\ (\bar{H}^i + \check{H}_K^i)\Delta\boldsymbol{p} \end{bmatrix} + \mathcal{Q}_{\mathbf{1}}^\intercal \begin{bmatrix} \check{H}_1^i\Delta\check{\boldsymbol{p}}_1 \\ \vdots \\ \check{H}_K^i\Delta\check{\boldsymbol{p}}_K \end{bmatrix} \\
&= \mathcal{Q}_{\mathbf{1}}^\intercal \begin{bmatrix} h_1^i(\hat{\boldsymbol{p}}_1) + H_1^i\Delta\boldsymbol{p} \\ \vdots \\ h_K^i(\hat{\boldsymbol{p}}_K) + H_K^i\Delta\boldsymbol{p} \end{bmatrix} + \mathcal{Q}_{\mathbf{1}}^\intercal \begin{bmatrix} \check{H}_1^i\Delta\check{\boldsymbol{p}}_1 \\ \vdots \\ \check{H}_K^i\Delta\check{\boldsymbol{p}}_K \end{bmatrix} && (60)\\
&= \mathcal{Q}_{\mathbf{1}}^\intercal \begin{bmatrix} h_1^i(\hat{\boldsymbol{p}}_1 + \Delta\boldsymbol{p}) \\ \vdots \\ h_K^i(\hat{\boldsymbol{p}}_K + \Delta\boldsymbol{p}) \end{bmatrix} + \mathcal{Q}_{\mathbf{1}}^\intercal \begin{bmatrix} \check{H}_1^i\Delta\check{\boldsymbol{p}}_1 \\ \vdots \\ \check{H}_K^i\Delta\check{\boldsymbol{p}}_K \end{bmatrix} && (61)\\
&= \mathcal{Q}_{\mathbf{1}}^\intercal \boldsymbol{h}^i\big(\hat{\mathbf{X}}_1 \oplus \Delta\boldsymbol{p}\big) + \mathcal{Q}_{\mathbf{1}}^\intercal \begin{bmatrix} \check{H}_1^i\Delta\check{\boldsymbol{p}}_1 \\ \vdots \\ \check{H}_K^i\Delta\check{\boldsymbol{p}}_K \end{bmatrix}. && (62)
\end{aligned}$$

Thus, with $\hat{N}_1^i + \delta N^i = \hat{N}_2^i$, it follows that

$$\begin{aligned}\mathcal{Q}_{\mathbf{1}}^\intercal \boldsymbol{h}^i\big(\hat{\mathbf{X}}_1 \oplus \Delta\boldsymbol{p}\big) + \lambda\mathcal{R}_{\mathbf{1}}(\hat{N}_1^i + \delta N^i) \\ = \mathcal{Q}_{\mathbf{1}}^\intercal \boldsymbol{h}^i\big(\hat{\mathbf{X}}_2\big) + \lambda\mathcal{R}_{\mathbf{1}}\hat{N}_2^i + \mathcal{Q}_{\mathbf{1}}^\intercal \boldsymbol{\delta}_2,\end{aligned}$$

where $\boldsymbol{\delta}_2 \triangleq [\check{H}_1^i\Delta\check{\boldsymbol{p}}_1, \ldots, \check{H}_K^i\Delta\check{\boldsymbol{p}}_K]^\intercal$. With eqn. (38), $\|\Delta\check{\boldsymbol{p}}_k\| < \Delta_p$ and $|\epsilon_k^i| < \|\Delta\boldsymbol{p}\|^2/2\underline{\mathrm{D}}$, the bound in eqn. (45) can be derived. This conclusion can also apply to code measurements such that eqn. (44) is also valid.

By neglecting the perturbation $\boldsymbol{\delta}_2$ in eqn. (43-44), eqn. (42) can be obtained and this concludes the proof. Note that the definition of $\Delta\boldsymbol{p}$ in eqn. (59) is independent of i; therefore, the proof can be repeated for each satellite.

APPENDIX IV

This appendix proves Proposition 4. The proof will use the following symbols:

$$\mathbf{X}_1^* = \underset{\mathbf{X}\in\mathbb{R}^{n_s K}}{arg\,min} \|\boldsymbol{r}_1(\mathbf{X})\|^2, \quad \mathbf{X}_2^* = \underset{\mathbf{X}\in\mathbb{R}^{n_s K}}{arg\,min} \|\boldsymbol{r}_2(\mathbf{X})\|^2,$$

$$(\mathbf{X}_\star, \mathbf{N}_\star) \triangleq \underset{\mathbf{X}\in\mathbb{R}^{n_s K}, \mathbf{N}\in\mathbb{Z}^m}{arg\,min} \|\boldsymbol{r}_b(\mathbf{X}, \mathbf{N})\|^2,$$

and

$$\Delta\boldsymbol{p}_{12}^* = \underset{\Delta\boldsymbol{p}\in\mathbb{R}^3}{arg\,min} \|\boldsymbol{r}_2(\mathbf{X}_1^* \oplus \Delta\boldsymbol{p})\|^2.$$

Note that $\mathbf{X}_1^*$, $\mathbf{X}_2^*$ and $\mathbf{X}_\star$ are sets of trajectories. At each time t, with the definition in eqn. (3), any

trajectory $\mathbf{X}$ can be rewritten as $\mathbf{X} = [\mathbf{P}^\intercal, \mathbf{S}^\intercal]^\intercal$, where $\mathbf{P} = [\boldsymbol{p}^\intercal(t_1), \ldots, \boldsymbol{p}^\intercal(t_K)]^\intercal \in \mathbb{R}^{3K}$ and $\mathbf{S} = [\boldsymbol{s}^\intercal(t_1), \ldots, \boldsymbol{s}^\intercal(t_K)]^\intercal \in \mathbb{R}^{K(n_s-3)}$. Because by definition $\|\boldsymbol{r}_2\|^2$ (or $\|\boldsymbol{r}_b\|^2$) is independent of $\mathbf{S}$, the set $\mathbf{X}_2^*$ (or $\mathbf{X}_\star$) contains all trajectories with the same sequence of positions $\mathbf{P}_2^*$, but distinct values of $\mathbf{S}$. Each trajectory in $\mathbf{X}_2^*$ (or $\mathbf{X}_\star$) has the same value for $\|\boldsymbol{r}_2\|^2$ (or $\|\boldsymbol{r}_b\|^2$), but will be penalized differently by $\|\boldsymbol{r}_1\|^2$. Similarly, $\mathbf{X}_1^*$ is a trajectory set, each having the same shape $\mathbf{S}_1^*$, but with $\mathbf{P}$ shifted by a common vector $\Delta\boldsymbol{p}$ by Proposition 2. Each trajectory in $\mathbf{X}_1^*$ has the same value for $\|\boldsymbol{r}_1\|^2$ but different penalty for $\|\boldsymbol{r}_b\|^2$.

Proof 7: By the definition of $(\mathbf{X}_\star, \mathbf{N}_\star)$, it follows that for the float solution $\check{\mathbf{X}}$ defined in eqn. (12), $\forall(\Delta\boldsymbol{p}, \mathbf{N}) \in \mathbb{R}^3 \cup \mathbb{Z}^m$,

$$\|\boldsymbol{r}_b(\mathbf{X}_\star, \mathbf{N}_\star)\|^2 \leq \|\boldsymbol{r}_b(\check{\mathbf{X}} \oplus \Delta\boldsymbol{p}, \mathbf{N})\|^2. \tag{63}$$

Given $(\check{\mathbf{X}}, \check{\mathbf{N}})$ and $(\mathbf{X}_\star, \mathbf{N}_\star)$, the unique $(\Delta\boldsymbol{p}^\star, \mathbf{N}^\star)$ such that

$$\|\boldsymbol{r}_b(\check{\mathbf{X}} \oplus \Delta\boldsymbol{p}^\star, \mathbf{N}^\star)\|^2 = \|\boldsymbol{r}_b(\mathbf{X}_\star, \mathbf{N}_\star)\|^2, \tag{64}$$

is provided in Appendix III in the proof of Proposition 3. From Proposition 2 (with $\boldsymbol{\delta}_1 = \mathbf{0}$), it follows that

$$\|\boldsymbol{r}_1(\check{\mathbf{X}} \oplus \Delta\boldsymbol{p}^\star)\|^2 = \|\boldsymbol{r}_1(\check{\mathbf{X}})\|^2. \tag{65}$$

Similarly, by Proposition 2 (with $\boldsymbol{\delta}_1 = \mathbf{0}$), it can also be proven that

$$\|\boldsymbol{r}_1(\mathbf{X}_1^* \oplus \Delta\boldsymbol{p}_{12}^*)\|^2 = \|\boldsymbol{r}_1(\mathbf{X}_1^*)\|^2. \tag{66}$$

By Proposition 3 (with $\boldsymbol{\delta}_2 = \mathbf{0}$) and considering the identical optimality achieved by $\boldsymbol{p}_{12}^*$ and $\mathbf{X}_2^*$, it follows that

$$\|\boldsymbol{r}_2(\mathbf{X}_1^* \oplus \Delta\boldsymbol{p}_{12}^*)\|^2 = \|\boldsymbol{r}_2(\mathbf{X}_2^*)\|^2. \tag{67}$$

Since $\check{\mathbf{X}}$ is the float solution such that

$$\|\boldsymbol{r}_a(\check{\mathbf{X}})\|^2 \leq \|\boldsymbol{r}_a(\mathbf{X})\|^2, \quad \forall\mathbf{X} \in \mathbb{R}^{n_s K},$$

we have

$$\begin{aligned}&\|\boldsymbol{r}_1(\check{\mathbf{X}})\|^2 + \|\boldsymbol{r}_2(\check{\mathbf{X}})\|^2 \\ &\qquad \leq \|\boldsymbol{r}_1(\mathbf{X}_1^* \oplus \Delta\boldsymbol{p}_{12}^*)\|^2 + \|\boldsymbol{r}_2(\mathbf{X}_1^* \oplus \Delta\boldsymbol{p}_{12}^*)\|^2. \end{aligned}\tag{68}$$

Substituting eqn. (66-67) into (68), it follows that

$$\|\boldsymbol{r}_1(\check{\mathbf{X}})\|^2 + \|\boldsymbol{r}_2(\check{\mathbf{X}})\|^2 \leq \|\boldsymbol{r}_1(\mathbf{X}_1^*)\|^2 + \|\boldsymbol{r}_2(\mathbf{X}_2^*)\|^2.$$

By the definition of $\mathbf{X}_1^*$ and $\mathbf{X}_2^*$,

$$\begin{aligned}\|\boldsymbol{r}_1(\mathbf{X}_1^*)\|^2 &\leq \|\boldsymbol{r}_1(\mathbf{X})\|^2, \quad \forall\mathbf{X} \in \mathbb{R}^{n_s K}, \\ \|\boldsymbol{r}_2(\mathbf{X}_2^*)\|^2 &\leq \|\boldsymbol{r}_2(\mathbf{X})\|^2, \quad \forall\mathbf{X} \in \mathbb{R}^{n_s K}.\end{aligned}\tag{69}$$

Combining these three inequalities yields

$$\|\boldsymbol{r}_1(\check{\mathbf{X}})\|^2 = \|\boldsymbol{r}_1(\mathbf{X}_1^*)\|^2. \tag{70}$$

By the definition of $(\mathbf{X}_\star, \mathbf{N}_\star)$ it follows that

$$\|\boldsymbol{r}_b(\mathbf{X}_\star, \mathbf{N}_\star)\|^2 \leq \|\boldsymbol{r}_b(\mathbf{X}, \mathbf{N})\|^2, \quad \forall(\mathbf{X}, \mathbf{N}) \in \mathbb{R}^{n_s K} \times \mathbb{Z}^m. \tag{71}$$

With eqn. (69), (71) and $\|\boldsymbol{r}_1\|^2 + \|\boldsymbol{r}_b\|^2 = \|\boldsymbol{r}\|^2$, it follows that

$$\|\boldsymbol{r}_1(\mathbf{X}_1^*)\|^2 + \|\boldsymbol{r}_b(\mathbf{X}_\star, \mathbf{N}_\star)\|^2 \leq \|\boldsymbol{r}(\mathbf{X}, \mathbf{N})\|^2, \ \forall(\mathbf{X}, \mathbf{N}).$$

Then, it follows that

$$\|\boldsymbol{r}_1(\mathbf{X}_1^*)\|^2 + \|\boldsymbol{r}_b(\mathbf{X}_\star, \mathbf{N}_\star)\|^2 \leq \|\boldsymbol{r}(\mathbf{X}^*, \mathbf{N}^*)\|^2. \tag{72}$$

From eqn. (64), (65) and (70),

$$\|\boldsymbol{r}_1(\check{\mathbf{X}} \oplus \Delta\boldsymbol{p}^\star)\|^2 + \|\boldsymbol{r}_b(\check{\mathbf{X}} \oplus \Delta\boldsymbol{p}^\star, \mathbf{N}^\star)\|^2 \leq \|\boldsymbol{r}(\mathbf{X}^*, \mathbf{N}^*)\|^2, \tag{73}$$

i.e.,

$$\|\boldsymbol{r}(\check{\mathbf{X}} \oplus \Delta\boldsymbol{p}^\star, \mathbf{N}^\star)\|^2 \leq \|\boldsymbol{r}(\mathbf{X}^*, \mathbf{N}^*)\|^2. \tag{74}$$

On the other hand, from eqn. (11) we have

$$\|\boldsymbol{r}(\mathbf{X}^*, \mathbf{N}^*)\|^2 \leq \|\boldsymbol{r}(\mathbf{X}, \mathbf{N})\|^2, \quad \forall\mathbf{X} \in \mathbb{R}^{n_s K}, \mathbf{N} \in \mathbb{Z}^m.$$

Thus, only equality can stand

$$\|\boldsymbol{r}(\check{\mathbf{X}} \oplus \Delta\boldsymbol{p}^\star, \mathbf{N}^\star)\|^2 = \|\boldsymbol{r}(\mathbf{X}^*, \mathbf{N}^*)\|^2,$$

and this concludes the proof.

APPENDIX V

This appendix proves Proposition 5 using similar techniques as were used for proving Proposition 4. In this proof, $\check{\mathbf{X}}$ and $\Delta\boldsymbol{p}^*$ are known and fixed.

Proof 8: Proposition 1 shows that the float solution $\check{\mathbf{X}}$ is equal to the integer-free solution, which optimizes the cost $\|\boldsymbol{r}_a(\mathbf{X})\|^2$ such that

$$\|\boldsymbol{r}_a(\check{\mathbf{X}})\|^2 \leq \|\boldsymbol{r}_a(\mathbf{X})\|^2, \quad \forall\mathbf{X} \in \mathbb{R}^{n_s K}.$$

Taking the norm of eqn. (30) after replacing $\boldsymbol{\delta}_1$ with (41), it follows that

$$\begin{aligned}&\|\bar{\mathcal{Q}}_1^\intercal \left(\boldsymbol{h}^i(\check{\mathbf{X}} \oplus \Delta\boldsymbol{p}^\star) - \boldsymbol{\varphi}^i\right)\|^2_{\sigma_\varphi^2\mathbf{I}^-} \\ &= \|\bar{\mathcal{Q}}_1^\intercal \left(\boldsymbol{h}^i(\check{\mathbf{X}}) - \boldsymbol{\varphi}^i\right)\|^2_{\sigma_\varphi^2\mathbf{I}^-} \\ &+ 2\begin{bmatrix}\check{H}_1^i\Delta\boldsymbol{p}^\star + \epsilon_1^i \\ \vdots \\ \check{H}_K^i\Delta\boldsymbol{p}^\star + \epsilon_K^i\end{bmatrix}^\intercal \bar{\mathcal{Q}}_{\mathbf{1}}(\sigma_\varphi^2\mathbf{I}^-)^{-1}\bar{\mathcal{Q}}_{\mathbf{1}}^\intercal \left(\boldsymbol{h}^i(\check{\mathbf{X}}) - \boldsymbol{\varphi}^i\right) \\ &+ \left\|\bar{\mathcal{Q}}_1^\intercal \begin{bmatrix}\check{H}_1^i\Delta\boldsymbol{p}^\star + \epsilon_1^i \\ \vdots \\ \check{H}_K^i\Delta\boldsymbol{p}^\star + \epsilon_K^i\end{bmatrix}\right\|^2_{\sigma_\varphi^2\mathbf{I}^-}.\end{aligned}\tag{75}$$

Given the Gaussian noise assumptions, after convergence of the float solution optimization process, the residual $\bar{\mathcal{Q}}_{\mathbf{1}}^\intercal \left(\boldsymbol{h}^i(\check{\mathbf{X}}) - \boldsymbol{\varphi}^i\right)$ is a zero mean random variable modeled as Gaussian. Therefore, the expected value of eqn. (75) yields

$$\begin{aligned}&\boldsymbol{E}\left\{\|\bar{\mathcal{Q}}_1^\intercal \left(\boldsymbol{h}^i(\check{\mathbf{X}} \oplus \Delta\boldsymbol{p}^\star) - \boldsymbol{\varphi}^i\right)\|^2_{\sigma_\varphi^2\mathbf{I}^-}\right\} \leq \\ &\boldsymbol{E}\left\{\|\bar{\mathcal{Q}}_1^\intercal \left(\boldsymbol{h}^i(\check{\mathbf{X}}) - \boldsymbol{\varphi}^i\right)\|^2_{\sigma_\varphi^2\mathbf{I}^-}\right\} + \sigma_\varphi^{-2}K[B_1(\|\Delta\boldsymbol{p}^\star\|, \bar{v})]^2,\end{aligned}\tag{76}$$

because $\mathcal{Q} = [\mathcal{Q}_{\mathbf{1}}, \bar{\mathcal{Q}}_{\mathbf{1}}]$ allows that

$$\left\|\bar{\mathcal{Q}}_1^\intercal \begin{bmatrix}\check{H}_1^i\Delta\boldsymbol{p}^\star + \epsilon_1^i \\ \vdots \\ \check{H}_K^i\Delta\boldsymbol{p}^\star + \epsilon_K^i\end{bmatrix}\right\|^2_{\sigma_\varphi^2\mathbf{I}^-} \leq \left\|\mathcal{Q}^\intercal \begin{bmatrix}\check{H}_1^i\Delta\boldsymbol{p}^\star + \epsilon_1^i \\ \vdots \\ \check{H}_K^i\Delta\boldsymbol{p}^\star + \epsilon_K^i\end{bmatrix}\right\|^2_{\sigma_\varphi^2\mathbf{I}}$$

and $|\check{H}_k\Delta\boldsymbol{p}^\star + \epsilon_k^i| \le B_1(\Delta\boldsymbol{p}^\star, \bar{v})$, for any $k = 1, \ldots, K$. Note that an inequality analogous to ineq. (76) also applies to pseudorange measurements, i.e.,

$$\begin{aligned}&\boldsymbol{E}\left\{\|\bar{\mathcal{Q}}_1^\intercal\left(\boldsymbol{h}^i(\check{\mathbf{X}}\oplus\Delta\boldsymbol{p}^\star) - \boldsymbol{\rho}^i\right)\|^2_{\sigma_\rho^2\mathbf{I}^-}\right\} \le \\ &\boldsymbol{E}\left\{\|\bar{\mathcal{Q}}_1^\intercal\left(\boldsymbol{h}^i(\check{\mathbf{X}}) - \boldsymbol{\rho}^i\right)\|^2_{\sigma_\rho^2\mathbf{I}^-}\right\} + \sigma_\rho^{-2}K[B_1(\|\Delta\boldsymbol{p}^\star\|, \bar{v})]^2.\end{aligned} \tag{77}$$

Since a common-position-shift $\Delta\boldsymbol{p}$ will not cause any variation in the prior cost and the INS cost terms, it follows that

$$\begin{aligned}&\boldsymbol{E}\Big\{\|\boldsymbol{r}_1(\check{\mathbf{X}}\oplus\Delta\boldsymbol{p}^\star)\|^2 - \|\boldsymbol{r}_1(\check{\mathbf{X}})\|^2\Big\} \\ &\qquad\le m\left(\sigma_\rho^{-2} + \sigma_\varphi^{-2}\right)K[B_1(\|\Delta\boldsymbol{p}^\star\|, \bar{v})]^2,\end{aligned} \tag{78}$$

where m is the number of available satellites.

Similarly, with Proposition 3 and its proof, it can be derived that

$$\begin{aligned}&\boldsymbol{E}\left\{\|\boldsymbol{r}_b(\check{\mathbf{X}}\oplus\Delta\boldsymbol{p}^\star, \mathbf{N}^\star)\|^2 - \|\boldsymbol{r}_b(\mathbf{X}_\star, \mathbf{N}_\star)\|^2\right\} \\ &\qquad\le m\left(\sigma_\rho^{-2} + \sigma_\varphi^{-2}\right)K[B_1(\|\Delta\boldsymbol{p}^\star\|, \bar{v})]^2.\end{aligned} \tag{79}$$

Similarly by Proposition 2, it can also be proven that

$$\begin{aligned}&\boldsymbol{E}\left\{\|\boldsymbol{r}_1(\mathbf{X}_1^*\oplus\Delta\boldsymbol{p}_{12}^*)\|^2 - \|\boldsymbol{r}_1(\mathbf{X}_1^*)\|^2\right\} \\ &\qquad\le m\left(\sigma_\rho^{-2} + \sigma_\varphi^{-2}\right)K[B_1(\|\Delta\boldsymbol{p}_{12}^*\|, \bar{v})]^2.\end{aligned} \tag{80}$$

By Proposition 3,

$$\begin{aligned}&\boldsymbol{E}\left\{\|\boldsymbol{r}_2(\mathbf{X}_1^*\oplus\Delta\boldsymbol{p}_{12}^*)\|^2 - \|\boldsymbol{r}_2(\mathbf{X}_2^*)\|^2\right\} \\ &\qquad\le m\sigma_\rho^{-2}K[B_1(\|\Delta\boldsymbol{p}_{12}^*\|, \bar{v})]^2.\end{aligned} \tag{81}$$

Since $\check{\mathbf{X}}$ is the float solution such that

$$\|\boldsymbol{r}_a(\check{\mathbf{X}})\|^2 \le \|\boldsymbol{r}_a(\mathbf{X})\|^2, \quad \forall\mathbf{X} \in \mathbb{R}^{n_s K},$$

we have

$$\begin{aligned}&\|\boldsymbol{r}_1(\check{\mathbf{X}})\|^2 + \|\boldsymbol{r}_2(\check{\mathbf{X}})\|^2 \\ &\qquad\le \|\boldsymbol{r}_1(\mathbf{X}_1^*\oplus\Delta\boldsymbol{p}_{12}^*)\|^2 + \|\boldsymbol{r}_2(\mathbf{X}_1^*\oplus\Delta\boldsymbol{p}_{12}^*)\|^2.\end{aligned} \tag{82}$$

With ineq. (66-67) and (82), it follows that

$$\begin{aligned}&\boldsymbol{E}\Big\{\|\boldsymbol{r}_1(\check{\mathbf{X}})\|^2 + \|\boldsymbol{r}_2(\check{\mathbf{X}})\|^2 - \|\boldsymbol{r}_1(\mathbf{X}_1^*)\|^2 - \|\boldsymbol{r}_2(\mathbf{X}_2^*)\|^2\Big\} \\ &\qquad\le m\left(2\sigma_\rho^{-2} + \sigma_\varphi^{-2}\right)K[B_1(\|\Delta\boldsymbol{p}_{12}^*\|, \bar{v})]^2.\end{aligned}$$

and then

$$\begin{aligned}&\boldsymbol{E}\left\{\|\boldsymbol{r}_1(\check{\mathbf{X}})\|^2 - \|\boldsymbol{r}_1(\mathbf{X}_1^*)\|^2\right\} \\ &\qquad\le m\left(2\sigma_\rho^{-2} + \sigma_\varphi^{-2}\right)K[B_1(\|\Delta\boldsymbol{p}_{12}^*\|, \bar{v})]^2,\end{aligned} \tag{83}$$

since $\|\boldsymbol{r}_2(\check{\mathbf{X}})\|^2 - \|\boldsymbol{r}_2(\mathbf{X}_2^*)\|^2 \ge 0$ is always true. From ineq. (78) and (83), it follows that

$$\begin{aligned}&\boldsymbol{E}\left\{\|\boldsymbol{r}_1(\check{\mathbf{X}}\oplus\Delta\boldsymbol{p}^\star)\|^2 - \|\boldsymbol{r}_1(\mathbf{X}_1^*)\|^2\right\} \le \\ &\qquad m\left(3\sigma_\rho^{-2} + 2\sigma_\varphi^{-2}\right)K[B_1(\Delta, \bar{v})]^2,\end{aligned}$$

where $\Delta \triangleq \max(\|\Delta\boldsymbol{p}^\star\|, \|\Delta\boldsymbol{p}_{12}^*\|)$. Along with the ineq. (79) and the inequality

$$\|\boldsymbol{r}_1(\mathbf{X}_1^*)\|^2 + \|\boldsymbol{r}_b(\mathbf{X}_\star, \mathbf{N}_\star)\|^2 \le \|\boldsymbol{r}(\mathbf{X}^*, \mathbf{N}^*)\|^2,$$

it follows that

$$\begin{aligned}&\boldsymbol{E}\{\|\boldsymbol{r}(\check{\mathbf{X}}\oplus\Delta\boldsymbol{p}^\star, \mathbf{N}^\star)\|^2\} \\ &= \boldsymbol{E}\left\{\|\boldsymbol{r}_1(\check{\mathbf{X}}\oplus\Delta\boldsymbol{p}^\star)\|^2 + \|\boldsymbol{r}_b(\check{\mathbf{X}}\oplus\Delta\boldsymbol{p}^\star, \mathbf{N}^\star)\|^2\right\} \\ &\le \boldsymbol{E}\left\{\|\boldsymbol{r}_1(\mathbf{X}_1^*)\|^2 + \|\boldsymbol{r}_b(\mathbf{X}_\star, \mathbf{N}_\star)\|^2\right\} \\ &\quad + m\left(4\sigma_\rho^{-2} + 3\sigma_\varphi^{-2}\right)K[B_1(\Delta, \bar{v})]^2.\end{aligned} \tag{84}$$

Following the steps from eqn. (71-72) it yields that

$$\begin{aligned}&\boldsymbol{E}\{\|\boldsymbol{r}(\check{\mathbf{X}}\oplus\Delta\boldsymbol{p}^\star, \mathbf{N}^\star)\|^2\} \\ &\le \boldsymbol{E}\{\|\boldsymbol{r}(\mathbf{X}^*, \mathbf{N}^*)\|^2\} + m\left(4\sigma_\rho^{-2} + 3\sigma_\varphi^{-2}\right)K[B_1(\Delta, \bar{v})]^2 \\ &= \boldsymbol{E}\{\|\boldsymbol{r}(\mathbf{X}^*, \mathbf{N}^*)\|^2\}(1 + C_3),\end{aligned}$$

where

$$C_3 = \frac{m\left(4\sigma_\rho^{-2} + 3\sigma_\varphi^{-2}\right)K[B_1(\Delta, \bar{v})]^2}{\boldsymbol{E}\{\|\boldsymbol{r}(\mathbf{X}^*, \mathbf{N}^*)\|^2\}}.$$

The optimum $\|\boldsymbol{r}(\mathbf{X}^*, \mathbf{N}^*)\|^2$ is referred as the *a-posteriori* variance factor in classical least square literature [47]. It can be shown that

$$\boldsymbol{E}\{\|\boldsymbol{r}(\mathbf{X}^*, \mathbf{N}^*)\|^2\} = (2K-1)m - 3,$$

where $(2K-1)m - 3 = (n_s K + 2Km - 3) - (n_s K + m)$ is the difference between the total number of measurements and the total dimension of unknown variables, which is also referred as the *degree-of-freedom*. Thus, it follows that

$$C_3 = \frac{m\left(4\sigma_\rho^{-2} + 3\sigma_\varphi^{-2}\right)K[B_1(\Delta, \bar{v})]^2}{(2K-1)m - 3}$$

Herein, both $\|\Delta\boldsymbol{p}^\star\|$ and $\|\Delta\boldsymbol{p}_{12}^*\|$ are upper bounded by Δ_f, so $\Delta \le \Delta_f$ and this concludes the proof.